Undulator A Characteristics and Specifications: Enhanced Capabilities

Roger J. Dejus, Barry Lai, Elizabeth R. Moog, and Efim Gluskin

Introduction

The undulator A for the Advanced Photon Source (APS) is a planar insertion device that will generate high-intensity x-ray radiation in the spectral range 3.2 keV to 45 keV by using the first, third, and fifth harmonics of radiation. The device has been optimized for the APS so that the variation in brilliance is small when tuning from one harmonic energy to the next. This has been achieved by an increase of the magnetic field for a given gap and by allowing a smaller minimum gap when installed in the storage ring.

This document describes the modification of the magnetic structure and the enhanced on-axis magnetic fields. The enhanced spectral performance is discussed and illustrated in tuning curves for the brilliance and the flux through apertures of different sizes. The increased power and power densities are described and also discussed in relation to selecting a proper sized aperture for an experiment. The spatial photon distribution is shown in figures at selected energies that clearly indicate the size of the central cone of radiation. This document is intended as a practical guide to aid in the design of beamlines for undulator A. Therefore, expanded sections describing the spatial photon distributions and the emitted power are included with graphs that can be used for accurate estimates of the beam size and power loads.

The spectral characteristics have been calculated[1] by the so-called Bessel function approximation using an effective magnetic field derived from model calculations of the magnetic field, and the power and power density have been calculated from the peak magnetic field. All spectral calculations include the emittance of the stored positron beam. In reality, there are random magnetic field errors that will reduce the ideal spectral characteristics shown here. The error tolerances specified for undulator A were chosen so the brilliance of the third harmonic will be at least 70% of the ideal, however.

This document is complementary to the technical bulletin ANL/APS/TB-3, which contains useful definitions and information about tapering of the device and the expected bandwidths of the first and third harmonics that are not repeated here. Other changes from TB-3 are revised values for the positron beam parameters and a correction to TB-3 Eq. 6.

[1] Program US, R. J. Dejus, unpublished.

Increased Magnetic Field

The undulator period length and the number of periods remain unchanged from the earlier design, and a summary of the technical specifications for undulator A is given in Table 1. The increase in the maximum attainable field arises from two separate changes. First, the undulator vendor[2] has agreed to build the undulators to a higher effective field specification (0.75 T at 11.5 mm gap, rather than 0.70 T). The higher field is reached by changing to a geometry in which the magnets and poles are wedge-shaped. Second, the vacuum chamber can be held to a higher standard of flatness than was anticipated earlier. The envelope allowed for the vacuum chamber need only be 0.2 mm larger than the nominal outside dimension (10.0 mm). Additional clearance must be considered because of the pole height variations of the undulator (0.2 mm) and a safety margin (0.1 mm). Extra clearance had previously been allowed between the upper and lower jaws of the undulator at the minimum gap to leave space for waviness in the vacuum chamber. Because much of that space is no longer need, the undulators will be able to close to a smaller minimum gap than previously planned (10.5 mm instead of 11.5 mm).

Model calculations of the magnetic design for undulator A have been performed using the three-dimensional magnetic modeling code Opera-3D.[3] The results are shown in Figures 1 and 2, in which the effective magnetic field B_{eff}, the effective deflection parameter K_{eff}, and the first harmonic energy E_1 are plotted as a function of the gap of the undulator. Table 2 gives the peak and effective fields for a device that meets but does not exceed the contracted field strength and the derived K_{eff} and E_1. The definition of K_{eff} is from the usual equation relating the deflection parameter and the magnetic field

$$K_{eff} = 0.934\, \lambda_u\, (\mathrm{cm}) B_{eff}\, (\mathrm{T}).$$

Note that the magnetic design for undulator A predicts a slightly larger field than what was specified. Nonetheless, the field strength used for the calculations herein is that given in Table 2, except where otherwise stated.

Parameters

The beam energy is 7.0 GeV and the beam current is 100 mA for all the results presented here. The energy bandwidth was set to the customary 0.1% for all calculations. We have also chosen 30.0 m from the center of the source to the aperture when calculating transmitted flux and power through a pinhole. This is a representative distance for the location of a first aperture to limit the size and the power of the beam transmitted down the beamline. The effective beam divergence scales approximately linearly with the distance from the source; thus it is straightforward to scale the numbers to the actual distance of interest for a particular beamline design. For a second-order correction, see Appendix A, which discusses the effect of the source size and other important source parameters for the APS.

[2] STI Optronics, 2755 Northup Way, Bellevue, WA 98004
[3] Vector Fields, 1700 N. Farnsworth Ave., Aurora, IL 60605

Brilliance Tuning Curves

The tuning curve for the on-axis brilliance is shown in Figure 3. With the enhanced magnetic field and the smaller minimum gap of 10.5 mm, there is now a continuous coverage from the lowest energy of 3.2 keV to 45 keV by using only the odd harmonics of radiation. In particular, the third harmonic is extended down to 10 keV and overlaps with the first harmonic before the brilliance drops dramatically. Similarly, the fifth harmonic is expected to provide the highest intensity above 20 keV.

The first harmonic has a peak brilliance fo 2.2×10^{18} at 5.3 keV and reduces by 8% at the minimum gap. The brilliance of the third harmonic is also in the 10^{18} range. The brilliance is expected to drop less than two orders of magnitude over the entire energy range up to 45 keV by using the radiation from the fifth harmonic.

The brilliance curves show the performance of an ideal device with no random field errors. The field errors for a real device will degrade the performance, and the brilliance for the higher harmonics will be reduced more that that for the lower. Undulator A has been specified with tight tolerances for the field errors (see Table 1) to ensure that the brilliance of the third harmonic attains at least 70% of its ideal value. Particularly important are the phase errors, which strongly correlate with the reduction of peak brilliance of the harmonics. The phase errors have been specified to be less than 8°, which translates into a predicted reduction of 2%, 16%, and 39% for the first, third, and fifth harmonic, respectively. Tests with an in-house prototype undulator achieved a third harmonic intensity of 85% of the ideal at a gap of 10.5 mm.

Flux through an Aperture

The tuning curves for a series of pinhole sizes located 30.0 m from the source are shown in Figure 4. The aspect ratio (2.5:1.0) for the pinhole was chosen to be the ratio of estimated beam divergence in the horizontal and vertical planes at high energies.

The tuning curves for the pinhole flux are similar to the tuning curves for the brilliance. For a 2.5 mm x 1.0 mm pinhole, we predict a maximum flux of 5.3×10^{14} (ph/s/0.1%bw) for the first harmonic at 4.2 keV, and the flux is expected to remain essentially constant when tuned to a lower energy. The cross-over energies for the harmonics are essentially unchanged, and the flux is expected to be 2×10^{14} (ph/s/0.1%bw) around 20 keV. The largest aperture (5.0 mm x 2.0 mm) extends beyond the central cone of radiation, and there is only a small gain in flux in comparison with the next-to-the-largest pinhole size.

The spectral flux at closed gap through the two largest apertures at 30.0 m is shown in Figure 5. The emittance for the APS introduces even harmonics in the spectrum and the tail on the low-energy side of the odd harmonics. For the 5.0 mm x 2.0 mm aperture, the peaks become broader and a smooth background intensity is observed.

Spatial Photon Distributions at Selected Energies

A series of calculations was made to illustrate the spatial distributions (irradiance) of photons, which may be helpful when designing beamlines. The central cone of radiation (half-peak intensity contour) is shown in the contour plots as the dark spot and the cross-section profiles along the horizontal and vertical directions are shown in adjacent figures. The given FWHMs of the profiles were determined from the data files and correlate well with the expected beam size as determined from Figure A1 (in the Appendix). Other contour lines are drawn for changes of one order of magnitude in the flux in units of ph/s/mm^2/0.1%bw at 30.0 m from the source.

Figure 6 shows the distributions at closed gap for a K value of 2.57 and a first harmonic energy of 3.25 keV. The first harmonic shows a distinct localized distribution with low intensity in the horizontal plane outside the central cone. There is also intensity in an outer ring around the first harmonic (except in the horizontal plane). The intensity distribution around the third harmonic shows a more complicated pattern. There is a substantial intensity in the horizontal plane in contrast to the pattern for the first harmonic. The fifth harmonic radiation pattern shows a well-defined central cone but also intensity in the horizontal plane. The features seen in these figures are elongated in the horizontal direction because of the larger emittance in the horizontal plane.

The set of contours shown in Figure 7 was obtained for a K value of 1.69, which corresponds to a gap of 14.5 mm and a first harmonic energy of 5.8 keV. The higher harmonics now show a cleaner pattern.

The contours with the first harmonic energy tuned to 8.0 keV are shown in Figure 8. Generally, the radiation pattern becomes smoother as the energy of the first harmonic increases. In most cases, the optimum flux is obtained by selecting the central cone of radiation. A larger flux may be obtained by increasing the size of the aperture, but this is at the expense of an increased transmitted power.

Power Considerations

The power loads may be substantial at small gaps. It is possible that the delivered undulators will have a field that is even higher than the model calculations predict. A model calculation was also performed at the new minimum gap of 10.5 mm, with magnets that have a remanent field B_r of 11.8 kG (instead of 11.6 kG), which is an upper limit for B_r for the finished, stabilized magnets. The peak field will then increase to 0.903 T, with an effective field of 0.888T. These values are considered as the highest field that might be achieved at a closed gap and might be used for conservative power calculations. For this effective field (K_{eff} is 2.74), the first harmonic energy would be 3.0 keV (rather than 3.2 keV).

In all the results presented here, we have used the specified peak field B_{peak} listed in Table 2 (with a corresponding maximum K value of 2.62 at closed gap) for calculating power and power densities. Figures 9a and 9b show the total emitted power and the peak heat flux at normal

incidence at 30.0 m from the source as a function of the gap and as a function of the first harmonic energy. The estimated total power is 5.3 kW, and the peak heat flux is 175 W/mm^2 at closed gap (by using a peak field of 0.903 T, we will obtain a "worst case" total emitted power of 6.0 kW and a peak heat flux of 180 W/mm^2 at 30.0 m). When plotted as a function of K, the peak heat flux shows an almost linear dependency on K, as can be seen in Figure 9c.

For beamline designs, it is also important to know the transmitted power through an aperture. The transmitted power through two apertures (2.5 mm x 1.0 mm, and 5.0 mm x 2.0 mm at 30.0 m) is shown in Figure 10a as a function of the gap setting and in Figure 10b as a function of the first harmonic energy. The 2.5 mm x 1.0 mm aperture corresponds approximately to the FWHM-size central cone of radiation at 30.0 m. Figure 10c shows the transmitted power as a function of K. The transmitted power through an aperture can be approximated by a straight line for all Ks except at very small values. In Figure 10, the two curves (apertures) represent two practical limiting cases: the small aperture corresponds to the FWHM-size of the central cone, whereas the large aperture extends slightly beyond the full size of the central cone.

The transmitted power through a small aperture (size on the order of the central cone) increases almost linearly with the area of the aperture. On the other hand, the flux at a fixed energy increases significantly up to about twice the area of the FWHM-size central cone; thereafter there is very little gain, and the gain is at the expense of the much larger transmitted power. Figures 11 to 19 show the variation of the flux through a pinhole of increasing size (aspect ratio 2.5:1.0) and the corresponding transmitted power at 30.0 m for several different energies (corresponding to different gaps of the undulator).

Figure 11 shows the flux fo 3.25 keV photons and the transmitted power (closed gap 10.5 mm), and Figure 12 gives the result for 5.76 keV photons (gap 14.5 mm). At 12 keV, it may be advantageous to use the first harmonic (n=1) rather than the third harmonic (n=3), despite the smaller flux as can be seen in Figure 14. X-rays at 12 keV may be obtained either from the first harmonic with undulator gap opened or from the third harmonic at a smaller gap. Similarly, around 20 keV, it is advantageous to use the third harmonic (at a large gap) rather than the fifth harmonic (at a small gap) as can be seen in Figure 16. At energies above 25 keV, the fifth harmonic provides the highest flux, and around 30 keV the trade-off between transmitted flux and power indicates that the fifth harmonic may be a better choice. At 40 keV, only the fifth harmonic provides a reasonably high flux.

Table 1. Undulator A parameters and specifications

Parameter	Value
Magnetic material	Nd-Fe-B
Pole material	Vanadium permendur
Period length, λ_u	3.30 cm
Number of periods, N[1]	72
Length, L	2.4 m
Minimum gap	10.5 mm
Maximum gap taper[2]	2 mrad
Deflection parameter, K_{eff} (K_{peak})[3]	2.57 (2.62)
Maximum field, B_{eff} (B_{peak})[3]	0.835 (0.849) T
First harmonic energy[3]	3.2 keV
rms peak magnetic field errors[4]	<0.5%
rms phase error	<8°

1) The number of periods was kept at 70 for all spectral calculations, so that the end poles were omitted. For power calculations, a conservative value of 72 periods was used.

2) Specified value; opens at downstream end.

3) Evaluated at minimum gap of 10.5 mm. Values are for the field that has been contractually agreed upon.

4) Specified at a gap of 11.5 mm.

Table 2. Peak and effective magnetic fields for undulator A.[1] The effective K value, K_{eff}, and the on-axis first harmonic energy E_1 are also given.

Gap (mm)	B_{peak}(T)	B_{eff} (T)	K_{eff}	E_1 (keV)
10.5[2]	0.849	0.835	2.57	3.27
11.0	0.803	0.791	2.44	3.55
11.5	0.760	0.750	2.31	3.84
12.0	0.720	0.712	2.19	4.14
13.0	0.647	0.641	1.98	4.78
14.0	0.582	0.578	1.78	5.45
14.5	0.553	0.549	1.69	5.80
15.0	0.525	0.522	1.61	6.15
16.0	0.474	0.472	1.45	6.85
17.0	0.429	0.427	1.32	7.56
18.0	0.388	0.387	1.19	8.24
19.0	0.351	0.350	1.08	8.92
20.0	0.318	0.317	0.977	9.55
25.0	0.196	0.196	0.604	11.9
30.0	0.121	0.121	0.373	13.2
35.0	0.0747	0.0746	0.230	13.7
40.0	0.0461	0.0461	0.142	14.0

1) These field values are for a device that meets but does not exceed the specified field in the midplane.

2) At the minimum gap of 10.5 mm, model calculations of the magnetic design predict a higher peak field (0.884 T) and a correspondingly higher effective field (0.869 T).

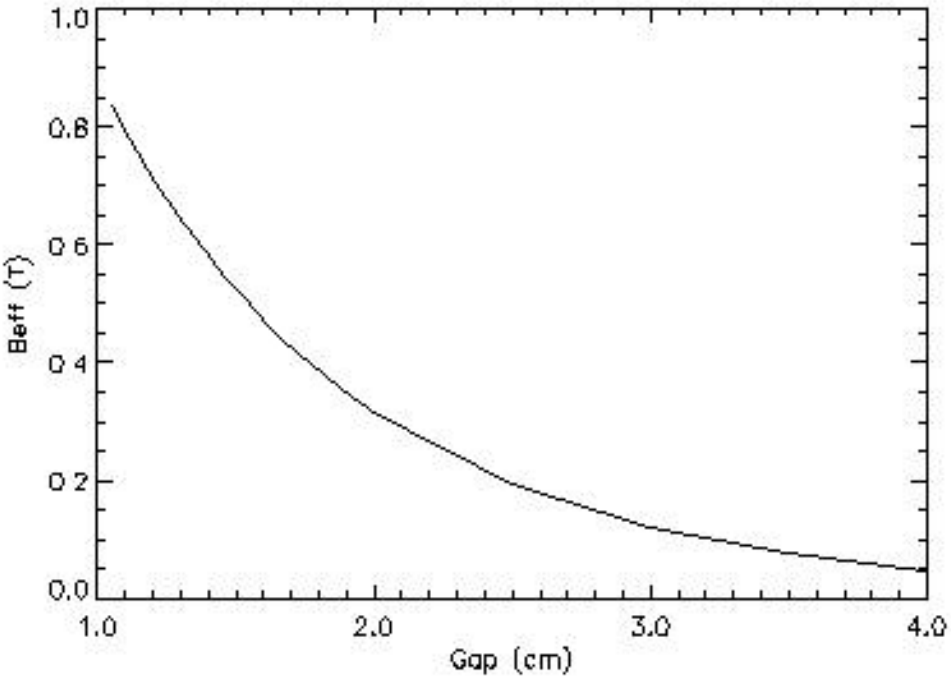

Figure 1. Effective magnetic field as a function of gap that meets but does not exceed the specification for undulator A.

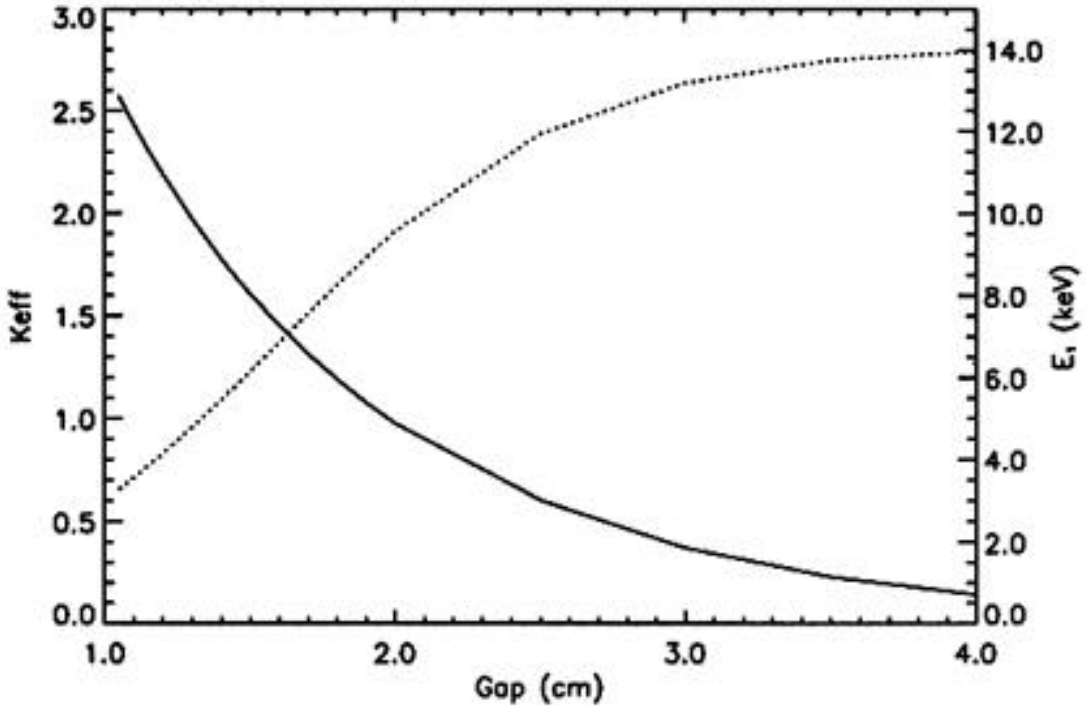

Figure 2. Effective K value and first harmonic energy as a function of gap.

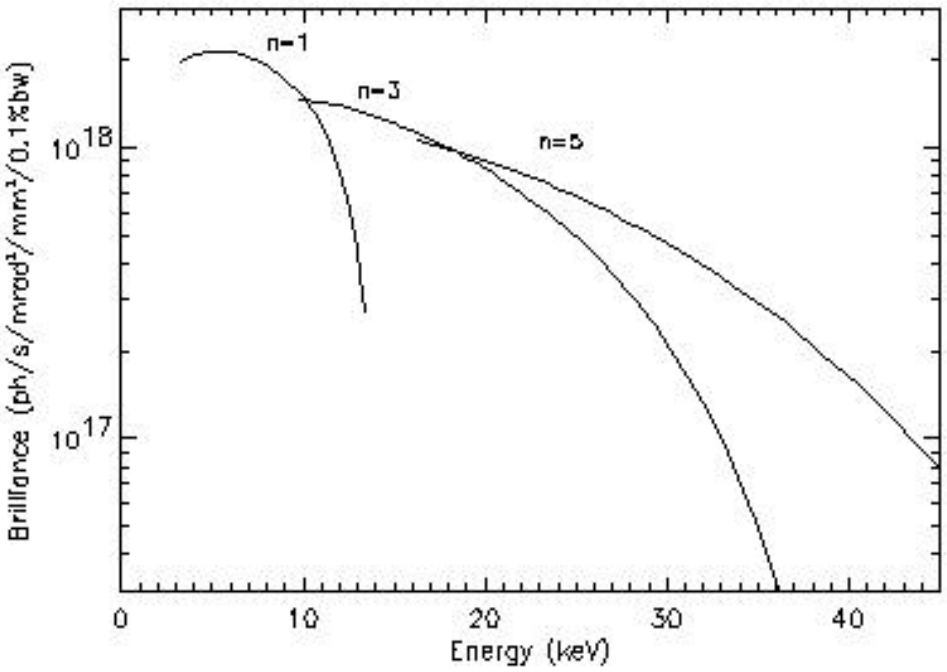

Figure 3. Tuning curves for the on-axis brilliance for the first three odd harmonics.

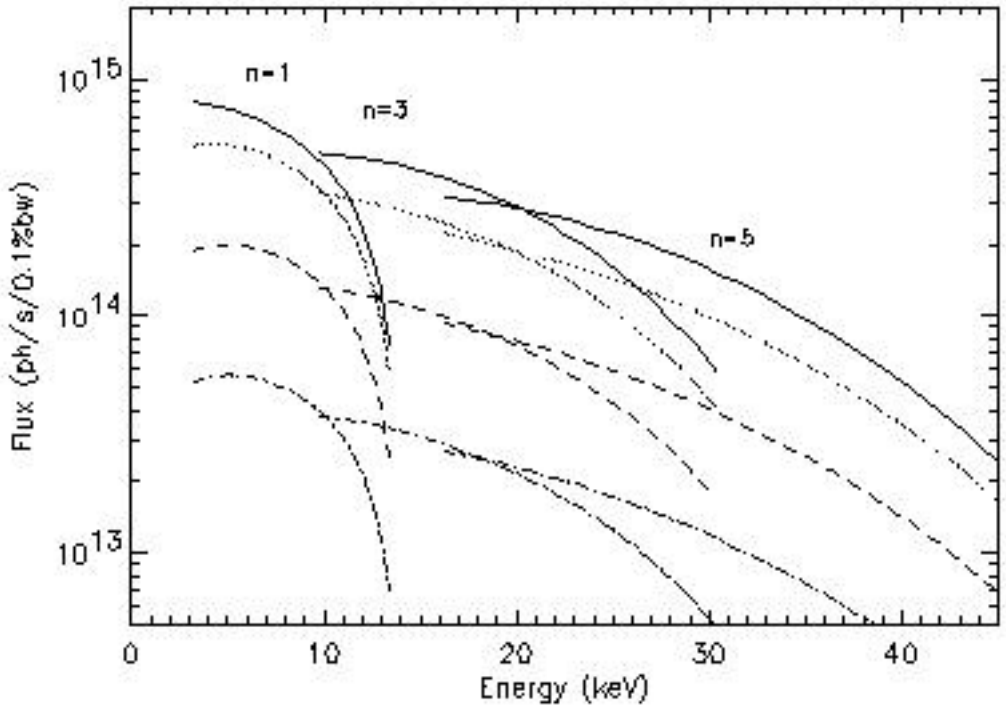

Figure 4. Tuning curves for the flux through a series of apertures of different sizes at 30.0 m from the source. Pinhole sizes are: 5.0 mm x 2.0 mm (solid), 2.5 mm x 1.0 mm (dotted), 1.25 mm x 0.5 mm (dashed), and 0.625 mm x 0.25 mm (dash-dotted).

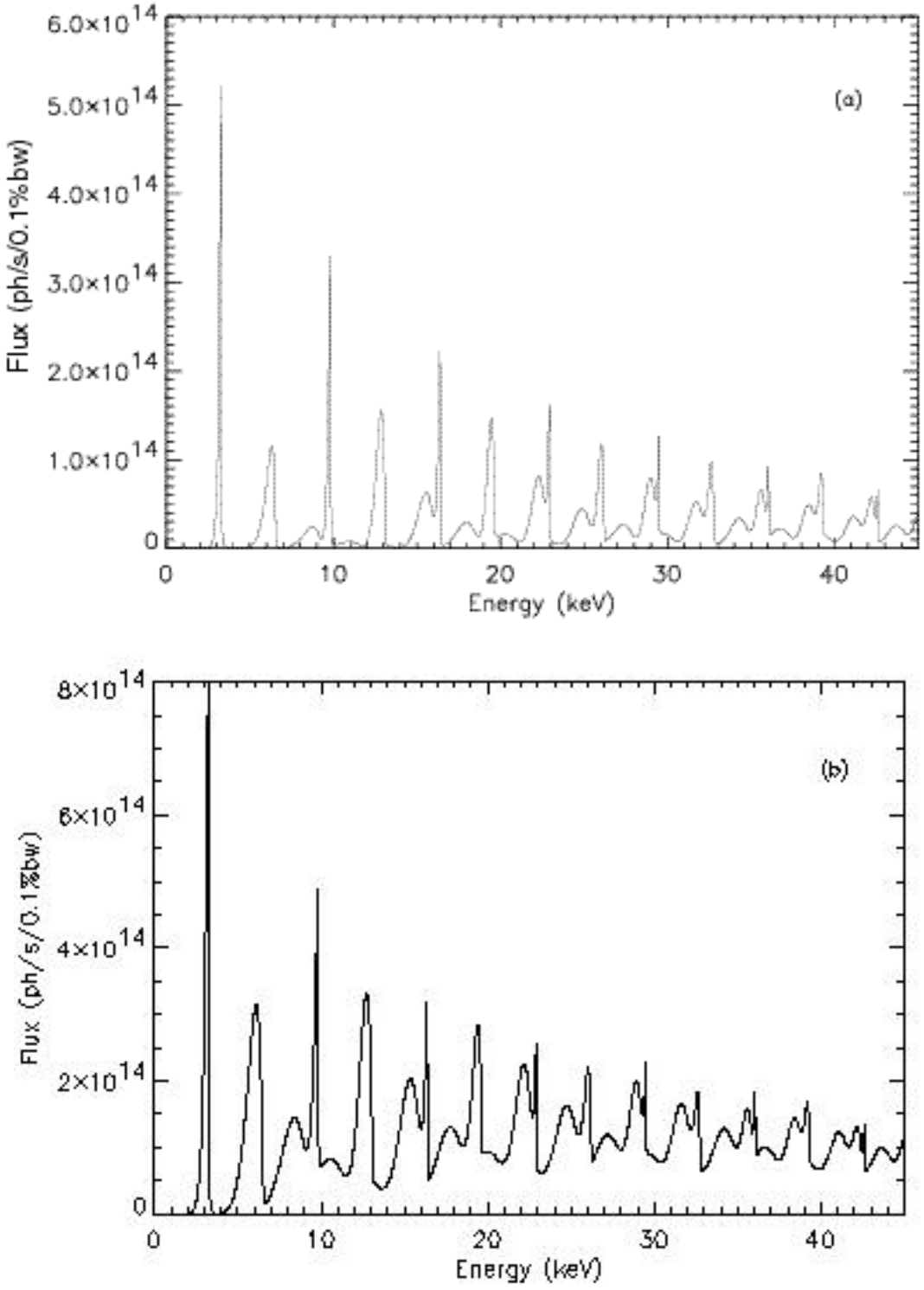

Figure 5. a) Spectral flux through a 2.5 x 1.0 mm aperture at 30.0 m from the source for a closed gap (10.5 mm, K_{eff} = 2.57). The peak intensity is 5.2 x 10^{14} ph/s/0.1%bw at the first harmonic energy (3.25 keV). b) Spectral flux through a 5.0 x 2.0 mm aperture. The peak intensity is 8.0 x 10^{14} ph/s/0.1%bw at the first harmonic energy (3.25 keV).

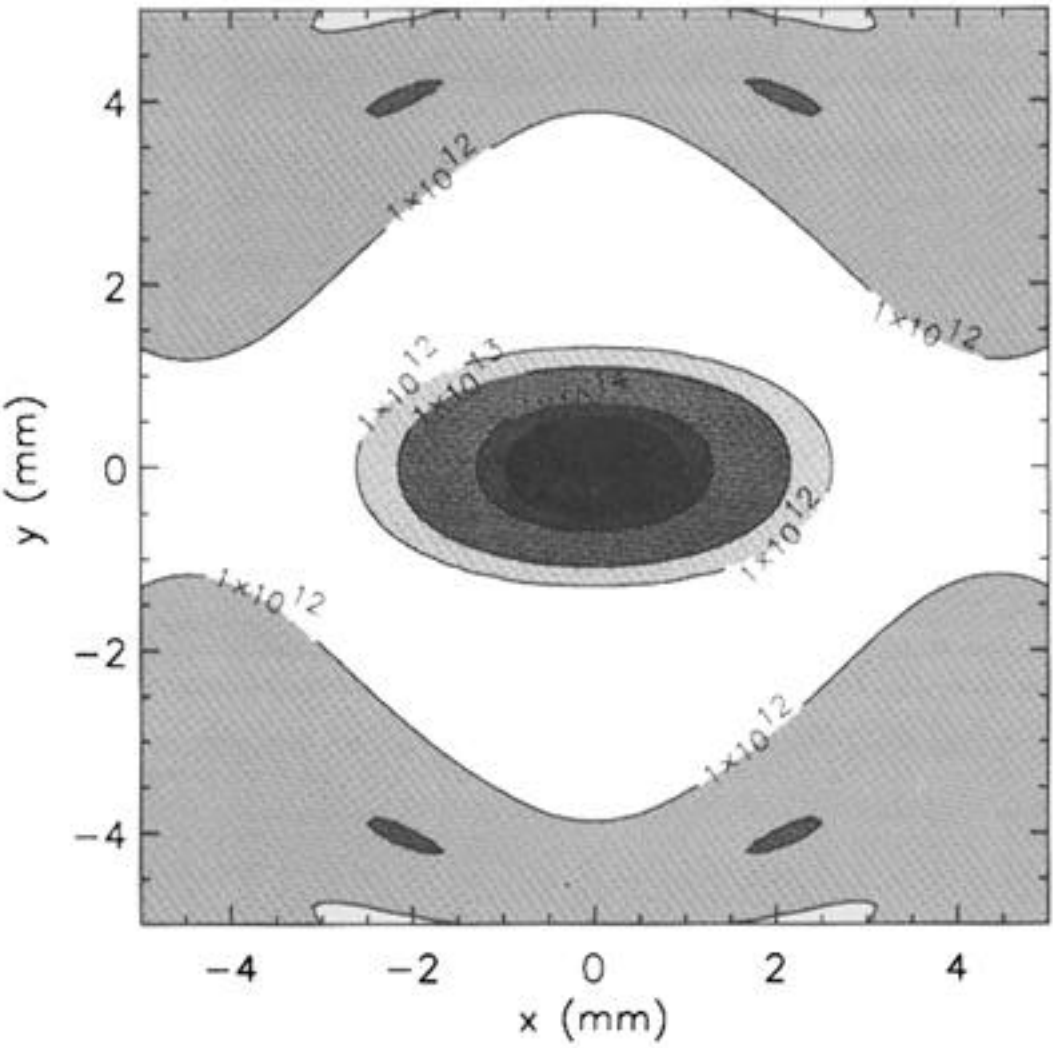

Figure 6a. Spatial photon distribution at 30.0 m from the source for a closed gap (10.5 mm, K_{eff} = 2.57) at the *first* harmonic energy (3.25 keV). The peak intensity is 3.39 x 10^{14} ph/s/mm^2/0.1%bw.

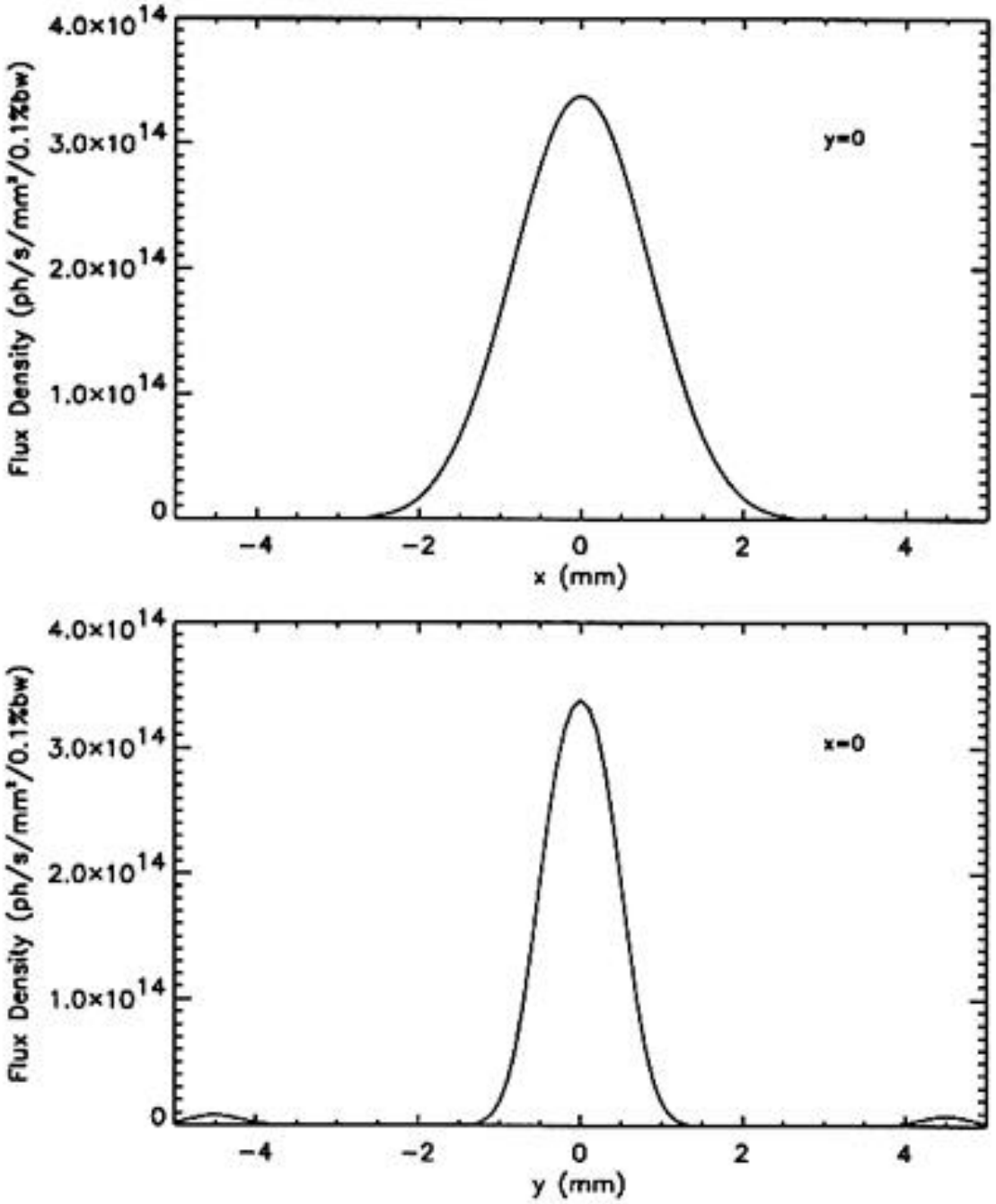

Figure 6b. Flux density cross-section profiles in the horizontal and vertical directions at the *first* harmonic energy (3.25 keV). The $FWHM_x$ is 1.96 mm, and the $FWHM_y$ is 1.10 mm.

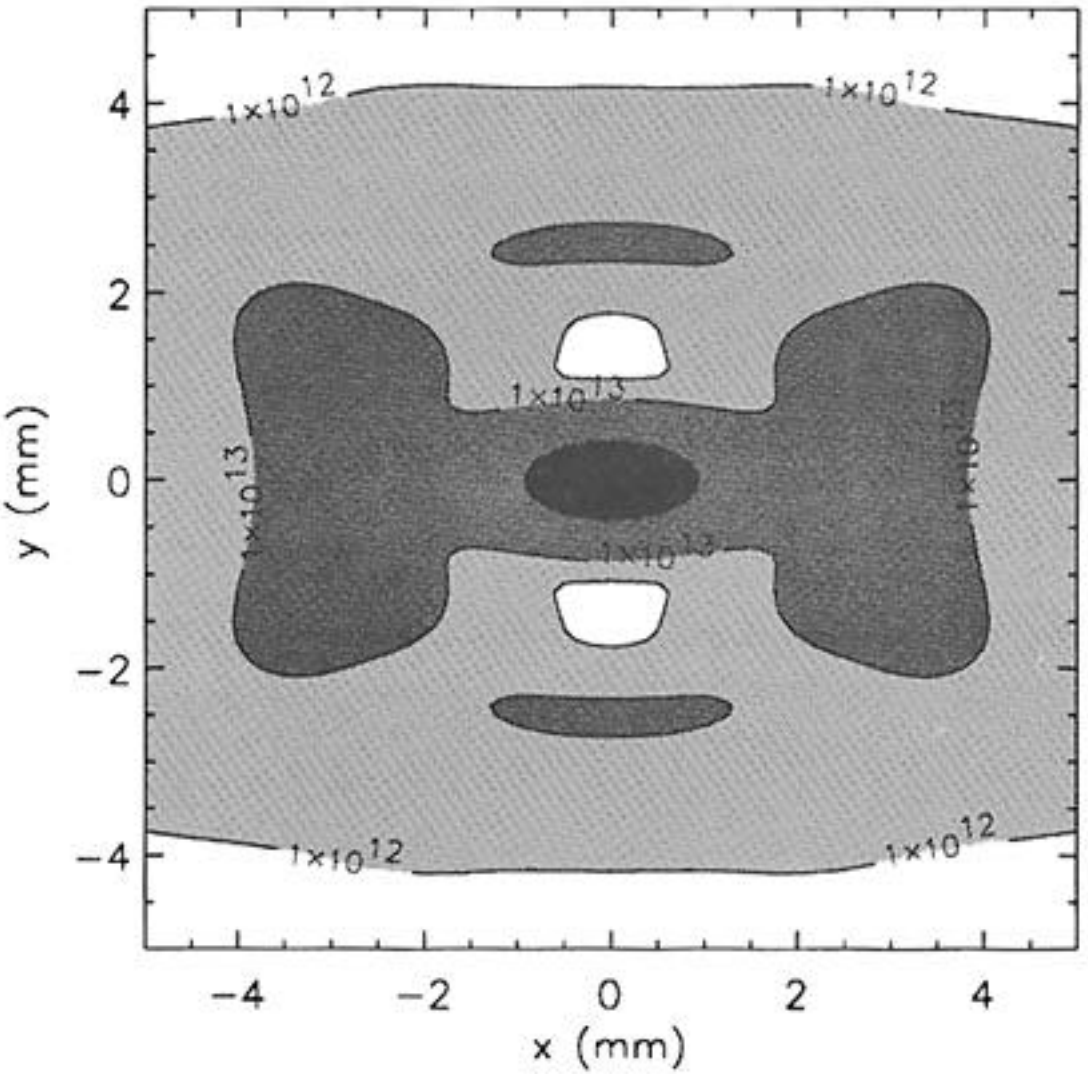

Figure 6c. Spatial photon distribution at 30.0 m from the source for a closed gap (10.5 mm, K_{eff} = 2.57) at the *third* harmonic energy (9.80 keV). The peak intensity is 2.51 x 10^{14} ph/s/mm^2/0.1%bw.

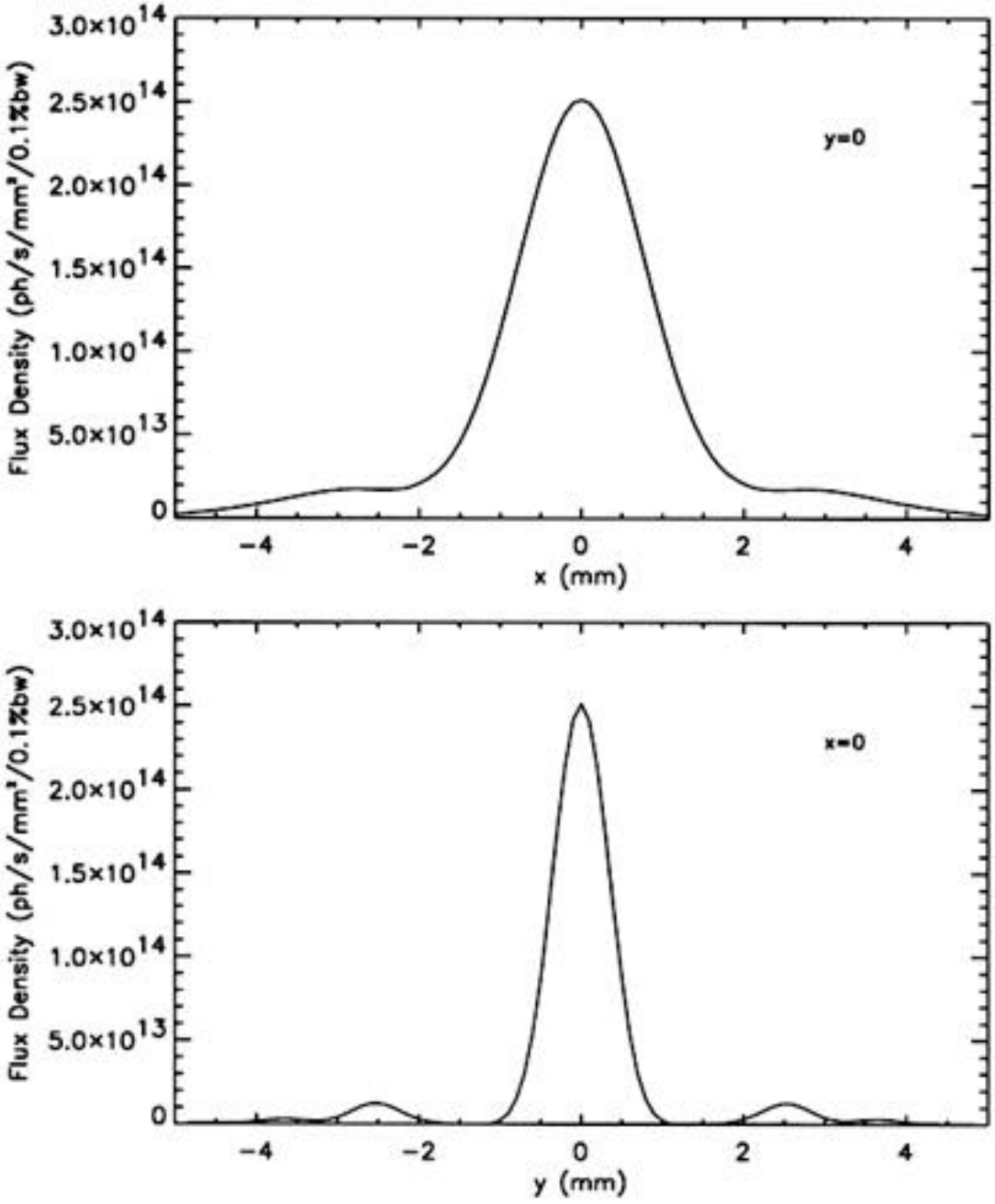

Figure 6d. Flux density cross-section profiles in the horizontal and vertical directions at the *third* harmonic energy (9.80 keV). The $FWHM_x$ is 1.86 mm, and the $FWHM_y$ is 0.82 mm.

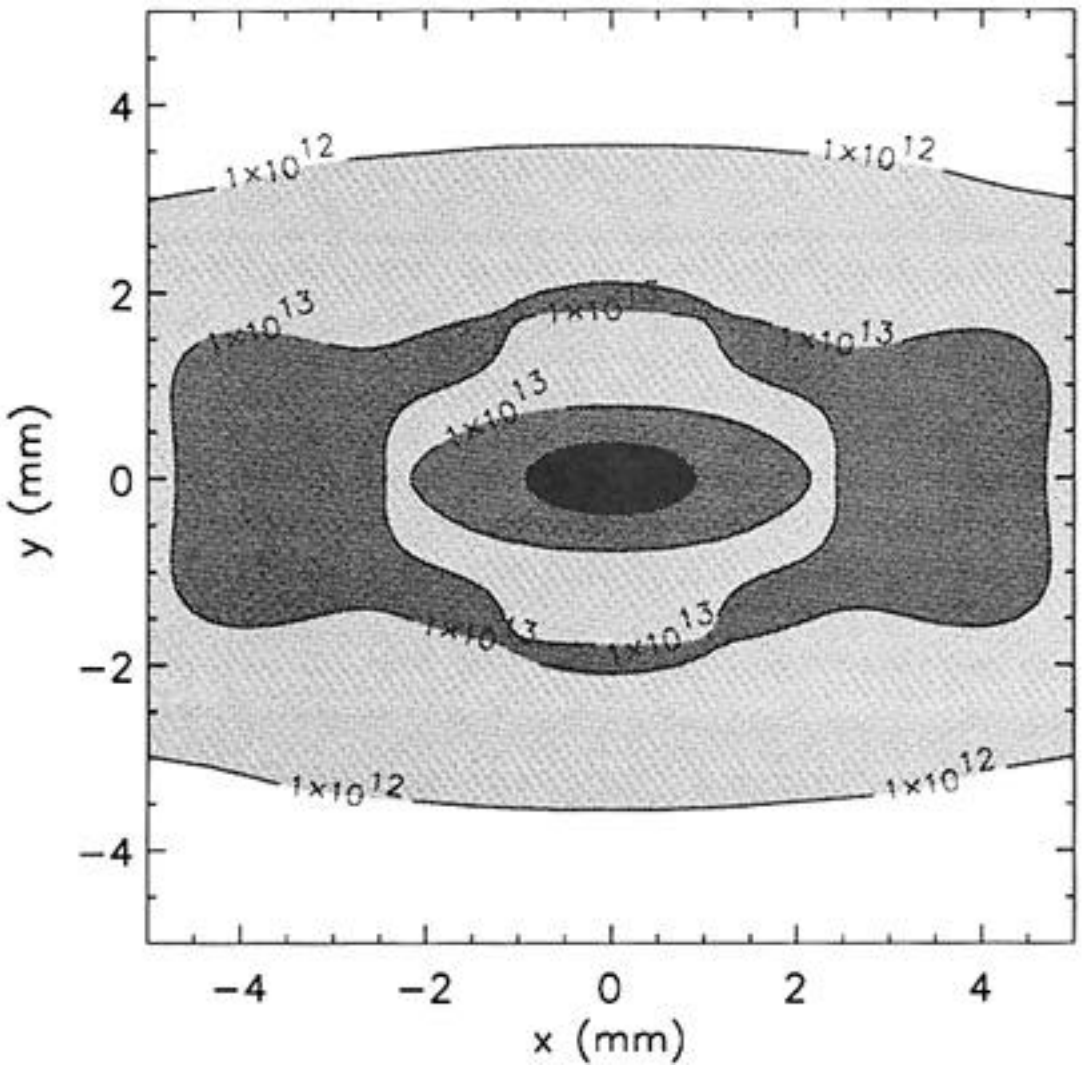

Figure 6e. Spatial photon distribution at 30.0 m from the source for a closed gap (10.5 mm, K_{eff} = 2.57) at the *fifth* harmonic energy (16.36 keV). The peak intensity is 1.78 x 10^{14} ph/s/mm^2/0.1%bw.

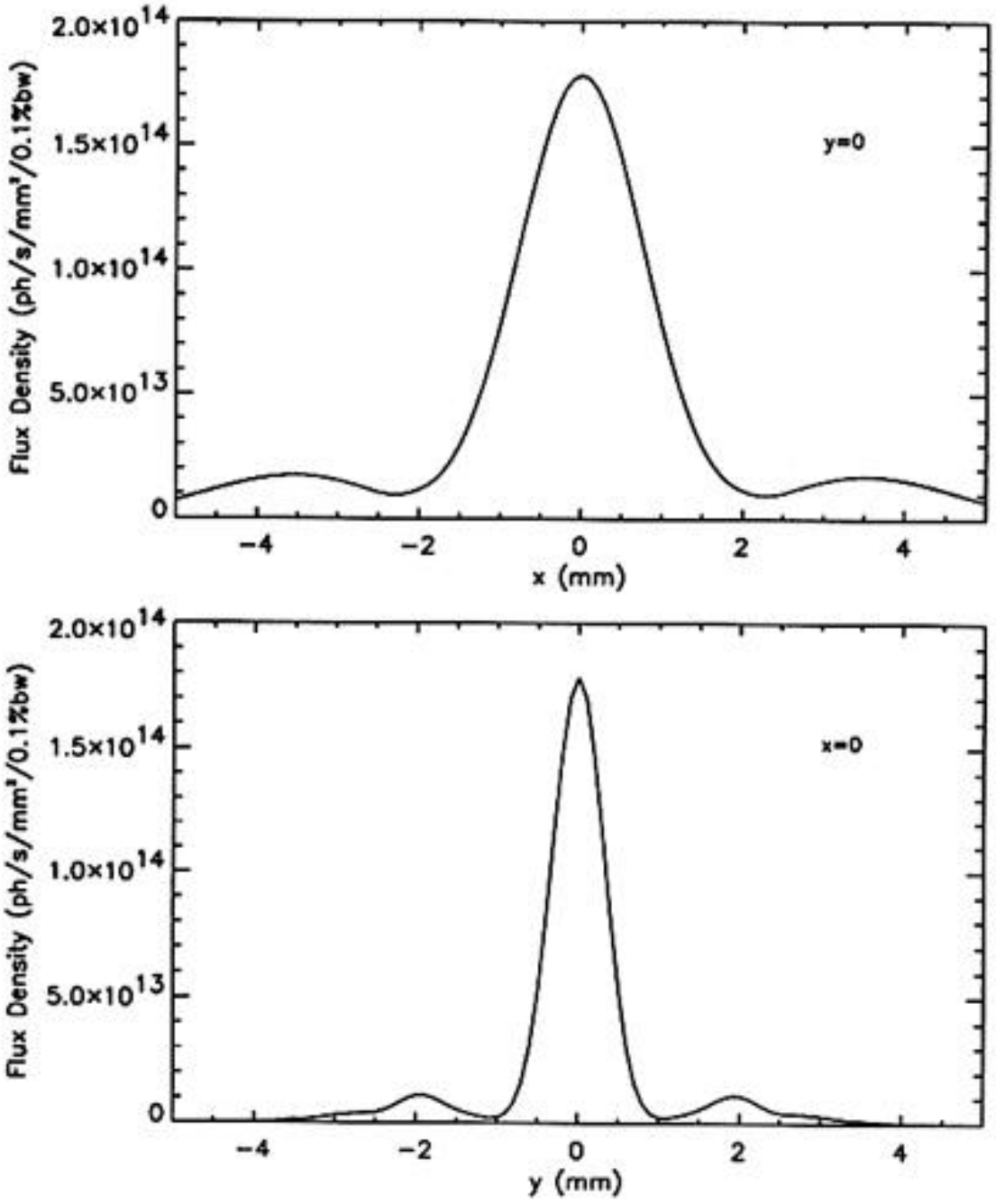

Figure 6f. Flux density cross-section profiles in the horizontal and vertical directions at the *fifth* harmonic energy (16.36 keV). The $FWHM_x$ is 1.83 mm, and the $FWHM_y$ is 0.76 mm.

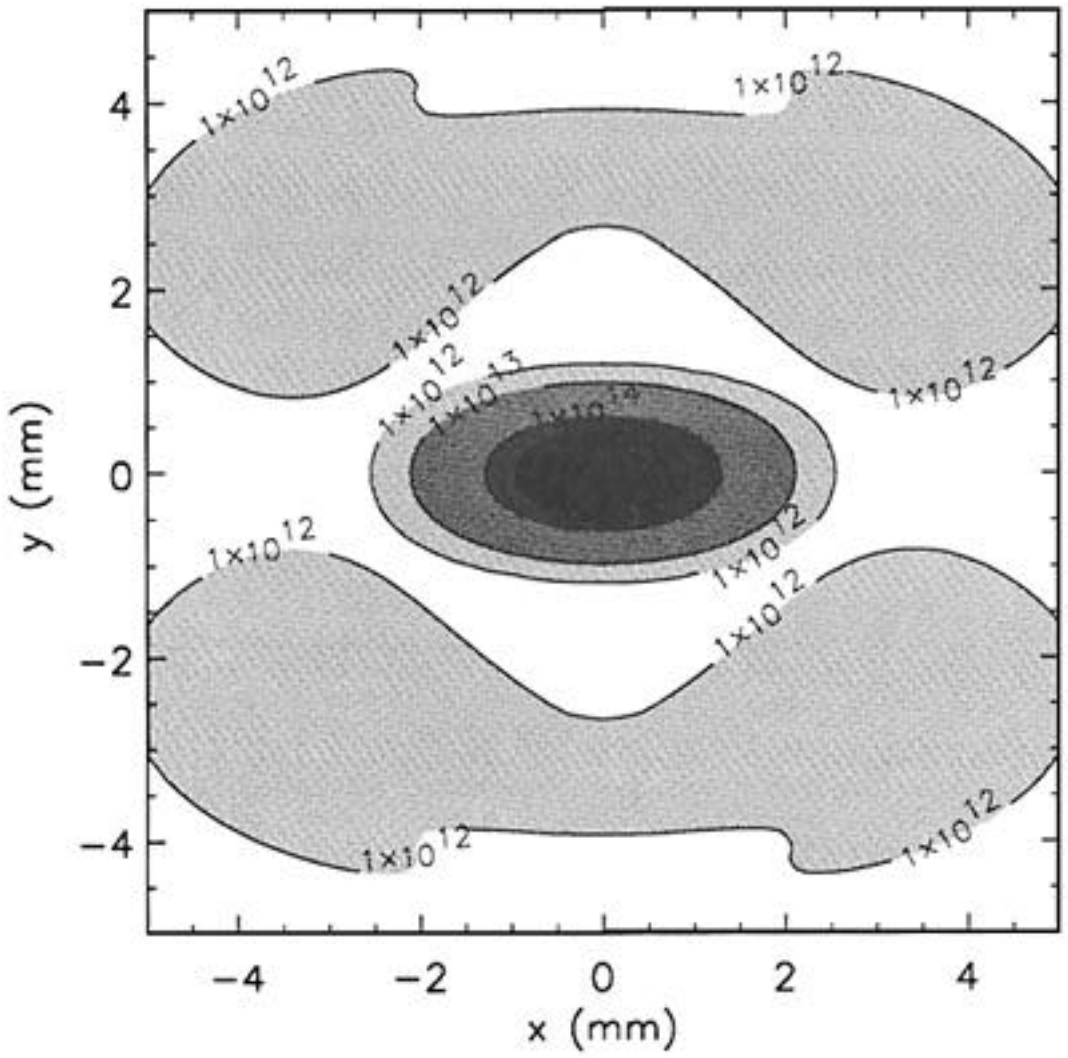

Figure 7a. Spatial photon distribution at 30.0 m from the source for K_{eff} = 1.69 (gap 14.5 mm) at the *first* harmonic energy (5.76 keV). The peak intensity is 3.66 x 10^{14} ph/s/mm^2/0.1%bw.

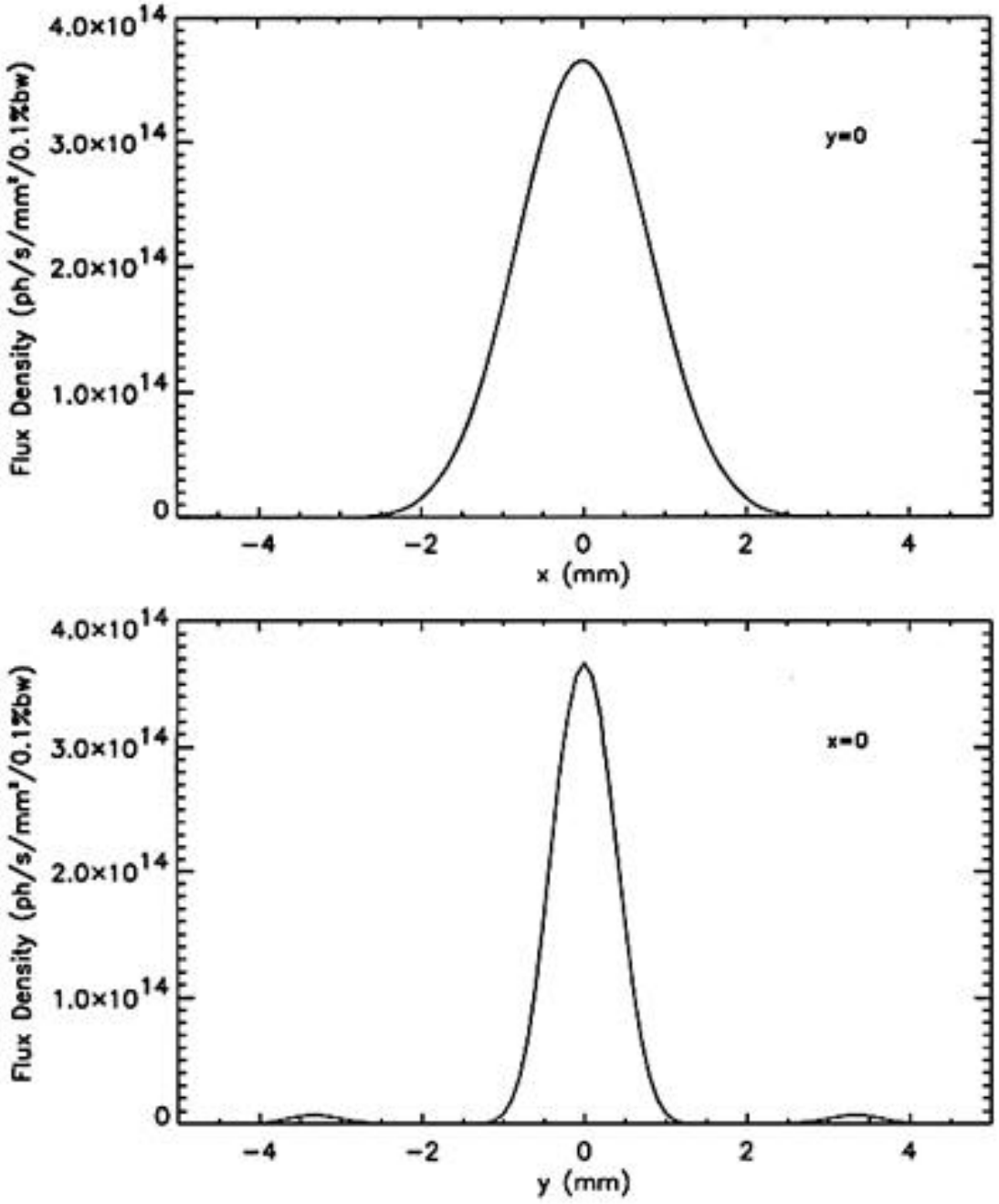

Figure 7b. Flux density cross-section profiles in the horizontal and vertical directions at the *first* harmonic energy (5.76 keV). The $FWHM_x$ is 1.89 mm, and the FWHM is 0.93 mm.

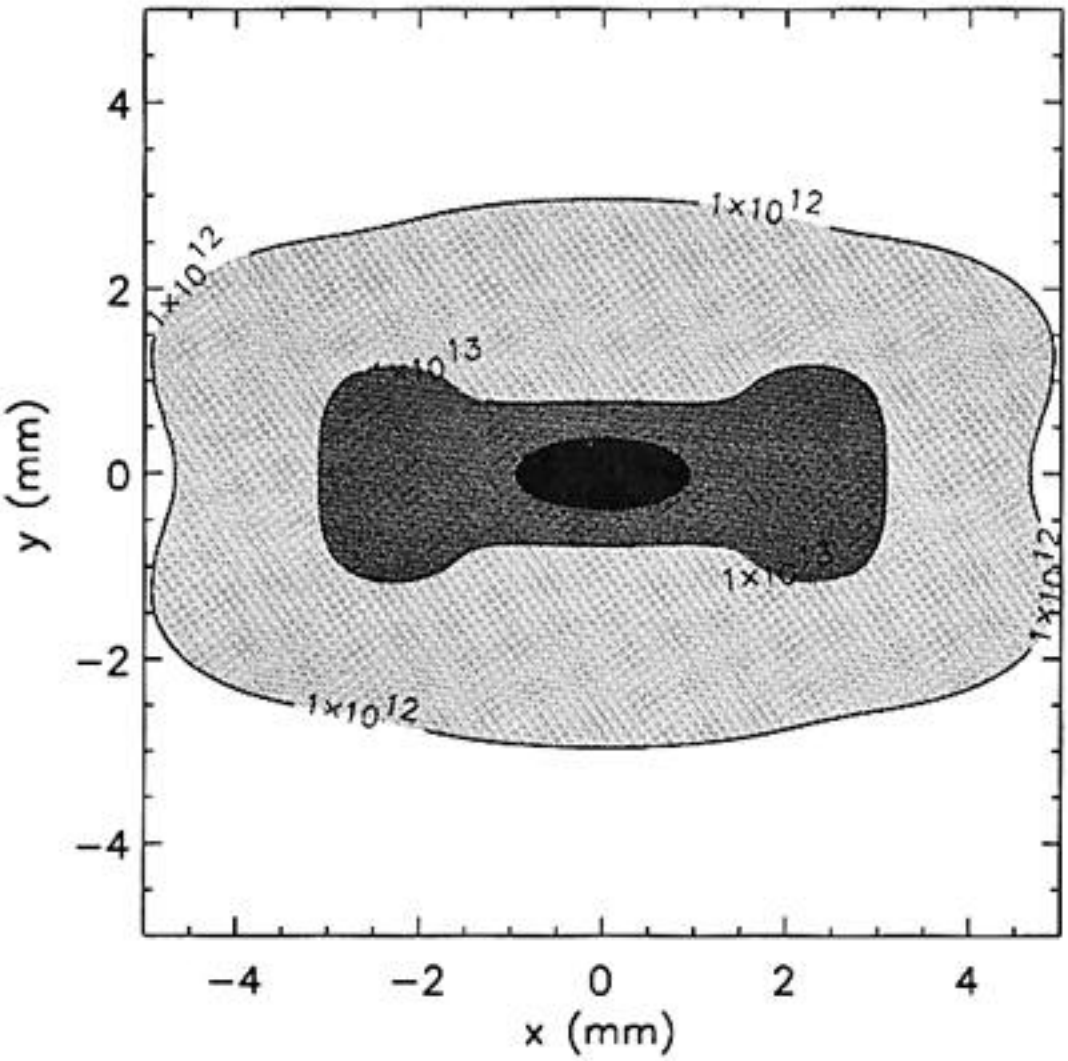

Figure 7c. Spatial photon distribution at 30.0 m from the source for K_{eff} = 1.69 (gap 14.5 mm) at the *third* harmonic energy (17.37 keV). The peak intensity is 1.78 x 10^{14} ph/s/mm^2/0.1%bw.

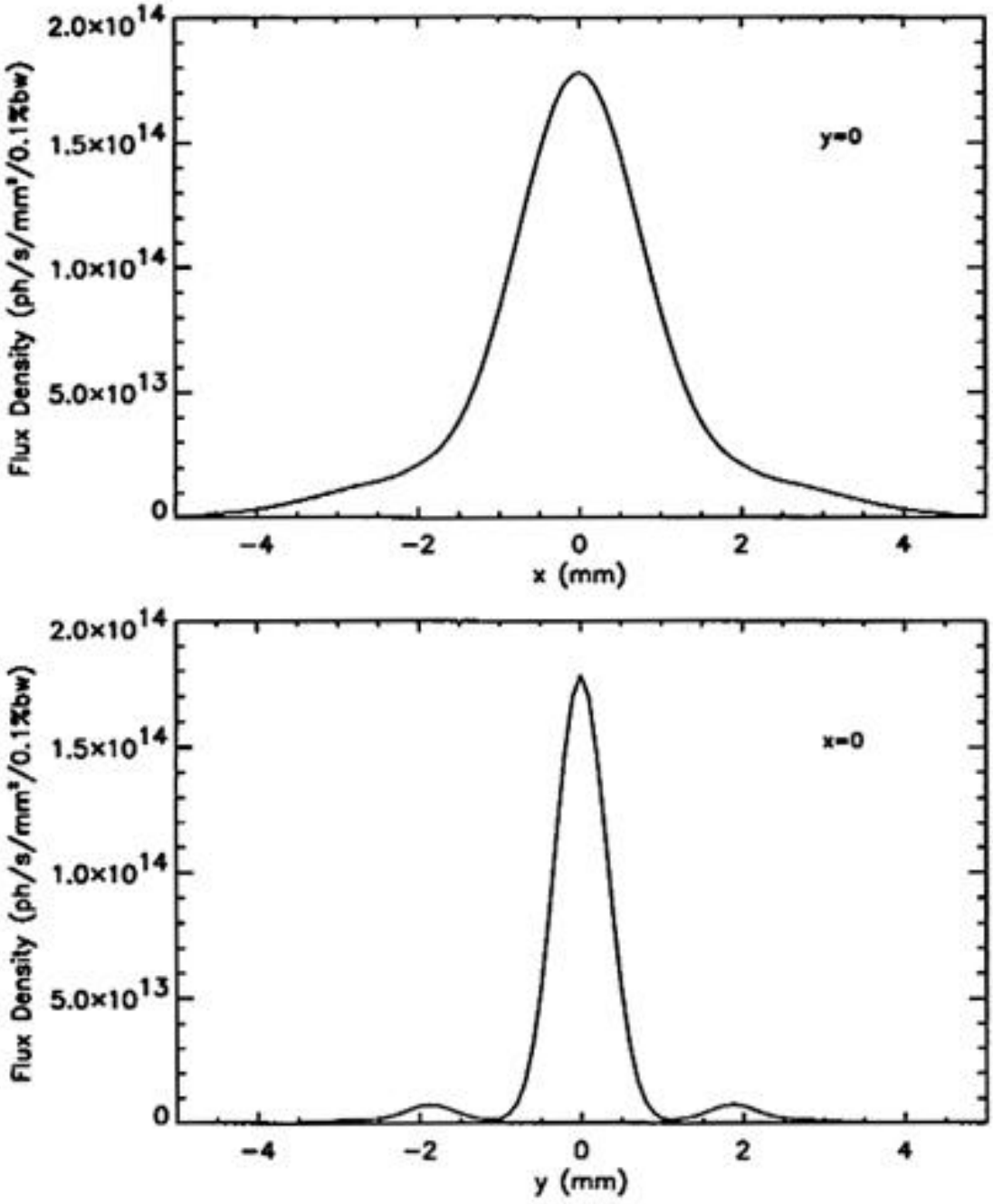

Figure 7d. Flux density cross-section profiles in the horizontal and vertical directions at the *third* harmonic energy (17.37 keV). The $FWHM_x$ is 1.90 mm, and the $FWHM_y$ is 0.76 mm.

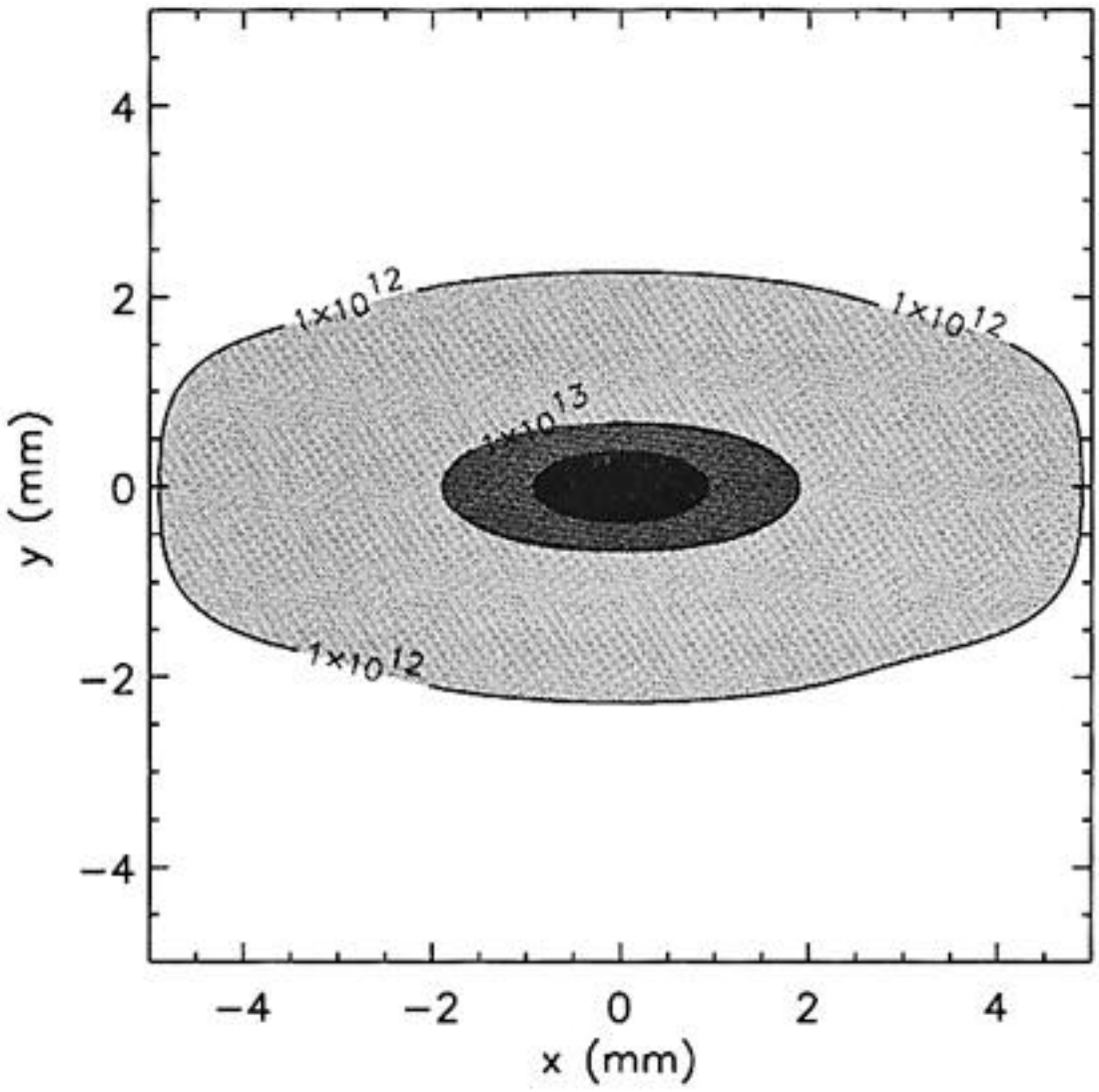

Figure 7e. Spatial photon distribution at 30.0 m from the source for K_{eff} = 1.69 (gap 14.5 mm) at the *fifth* harmonic energy (28.99 keV). The peak intensity is 8.65 x 10^{13} ph/s/mm^2/0.1%bw.

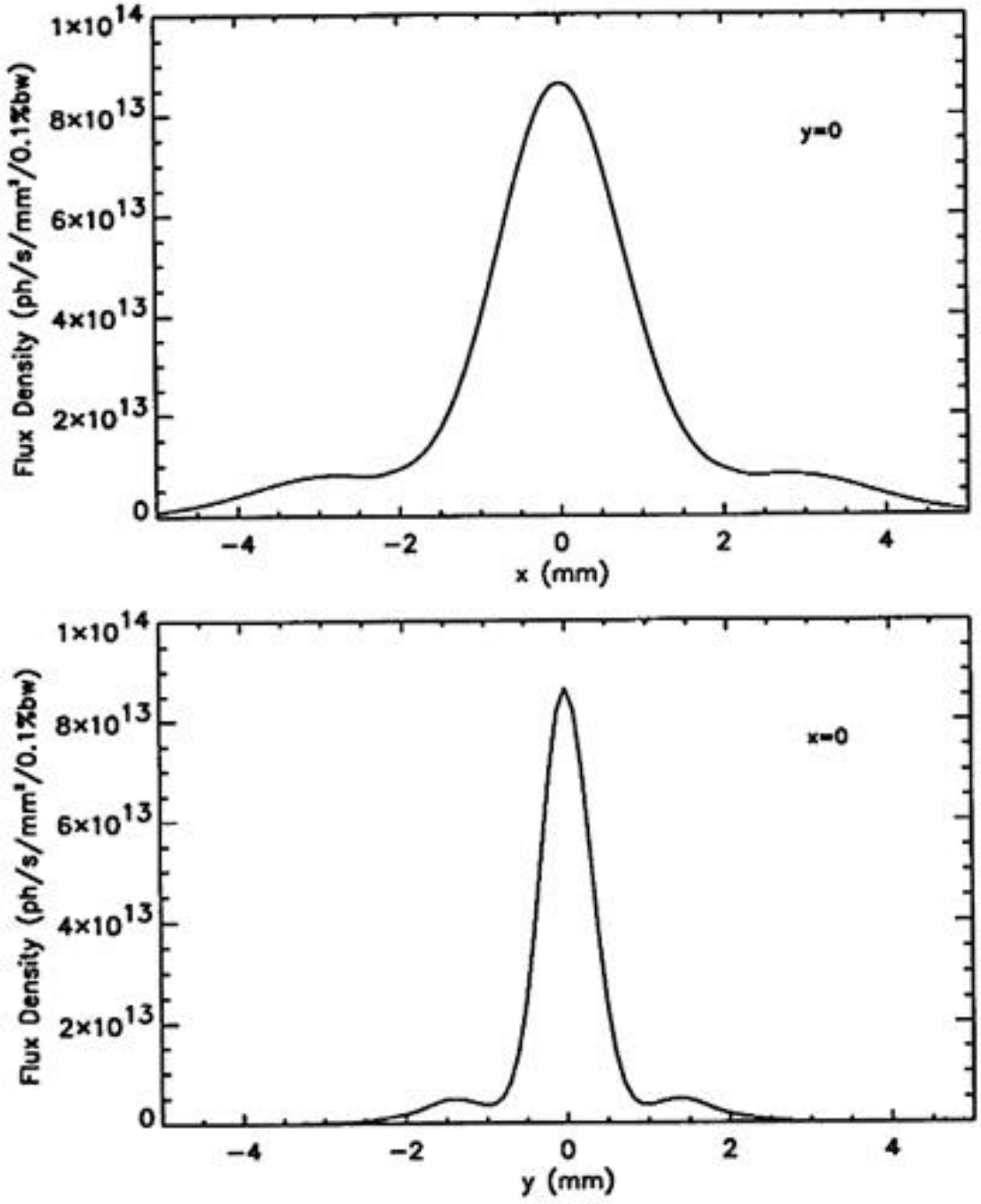

Figure 7f. Flux density cross-section profiles in the horizontal and vertical directions at the *fifth* harmonic energy (28.99 keV). The $FWHM_x$ is 1.87 mm, and the $FWHM_y$ is 0.73 mm.

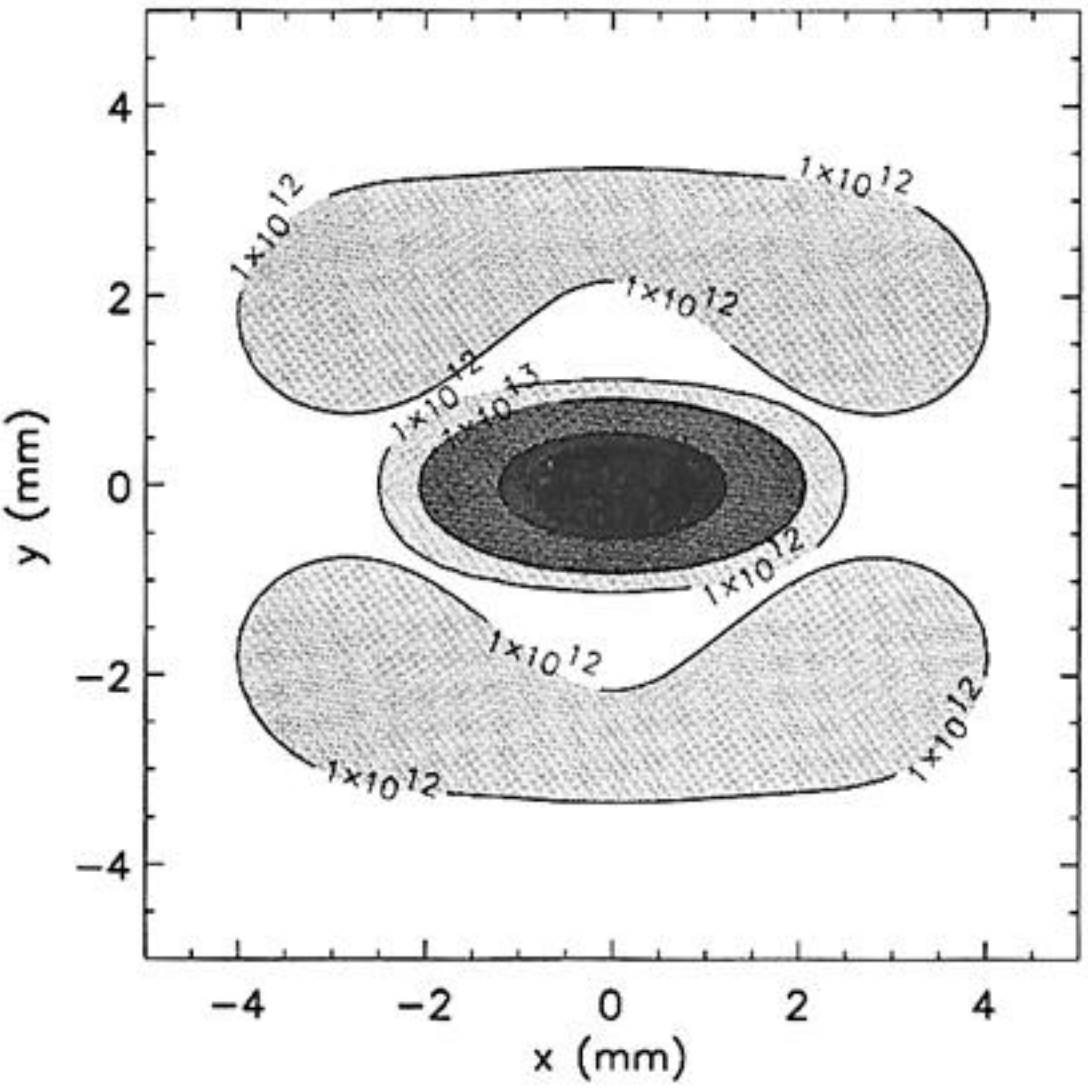

Figure 8a. Spatial photon distribution at 30.0 m from the source for K_{eff} = 1.22 (gap 17.8 mm) at the *first* harmonic energy (8.01 keV). The peak intensity is 3.25 x 10^{14} ph/s/mm^2/0.1%bw.

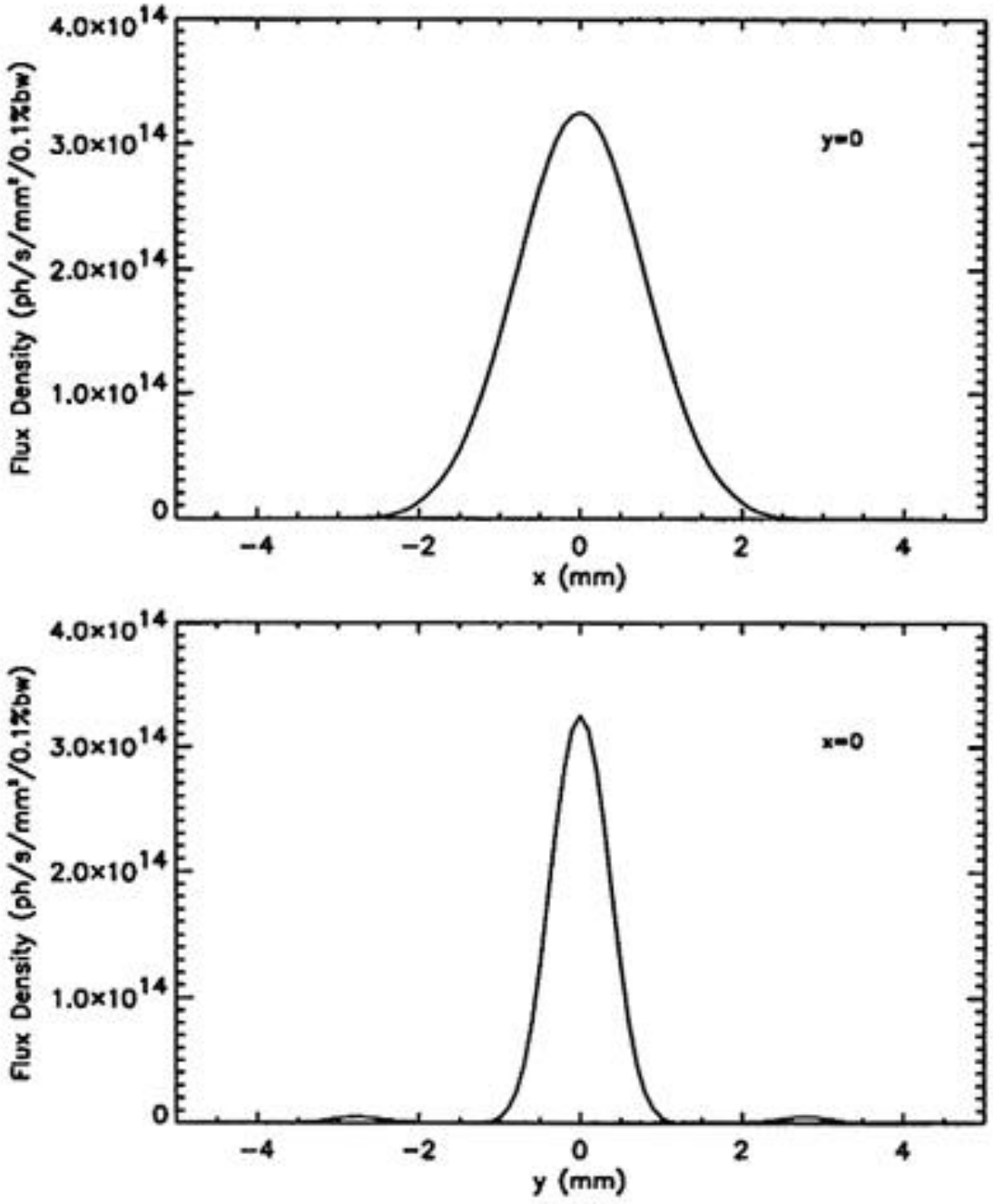

Figure 8b. Flux density cross-section profiles in the horizontal and vertical directions at the *first* harmonic energy (8.01 keV). The $FWHM_x$ is 1.87 mm, and the $FWHM_y$ is 0.87 mm.

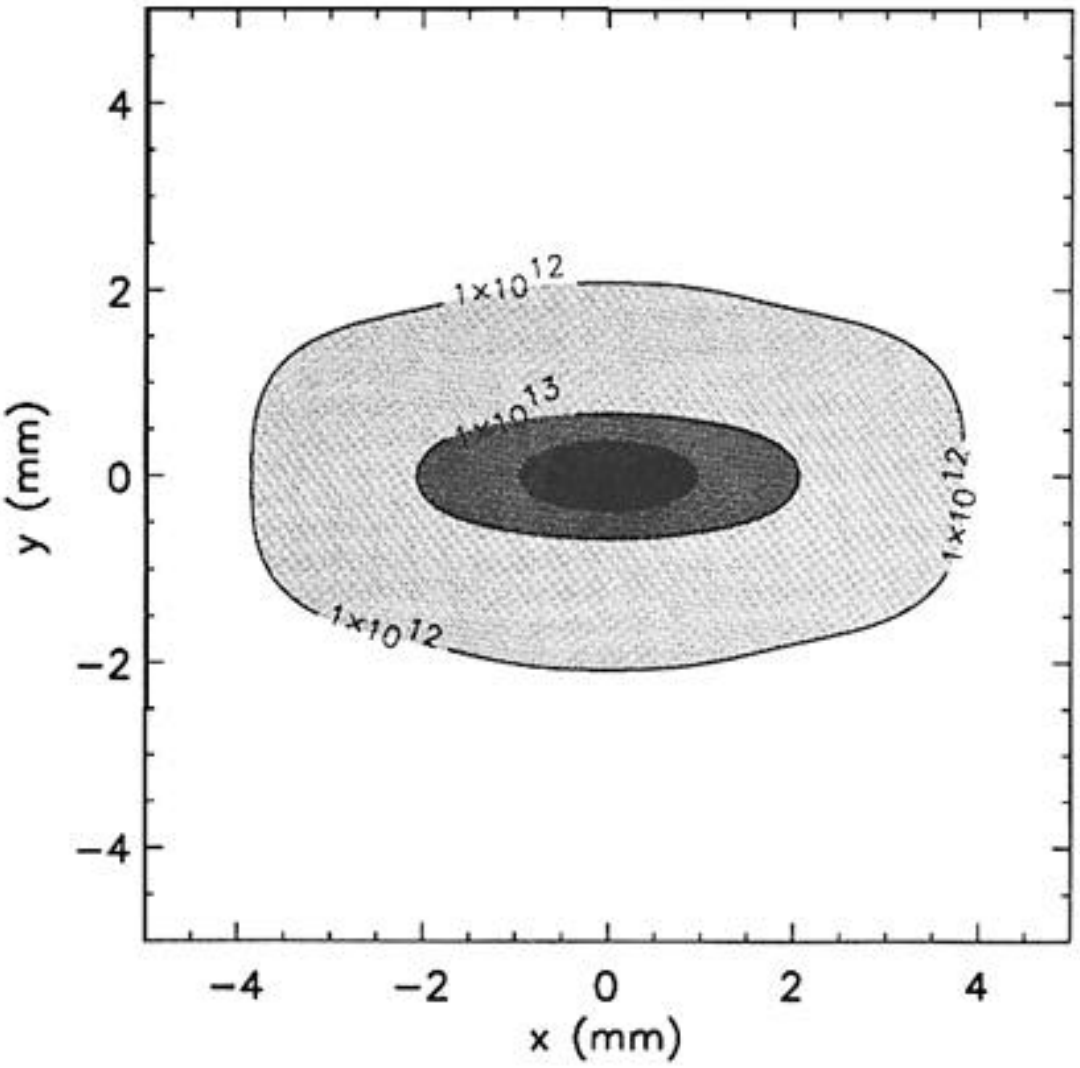

Figure 8c. Spatial photon distribution at 30.0 m from the source for K_{eff} = 1.22 (gap 17.8 mm) at the *third* harmonic energy (24.18 keV). The peak intensity is 9.25 x 10^{13} ph/s/mm^2/0.1%bw.

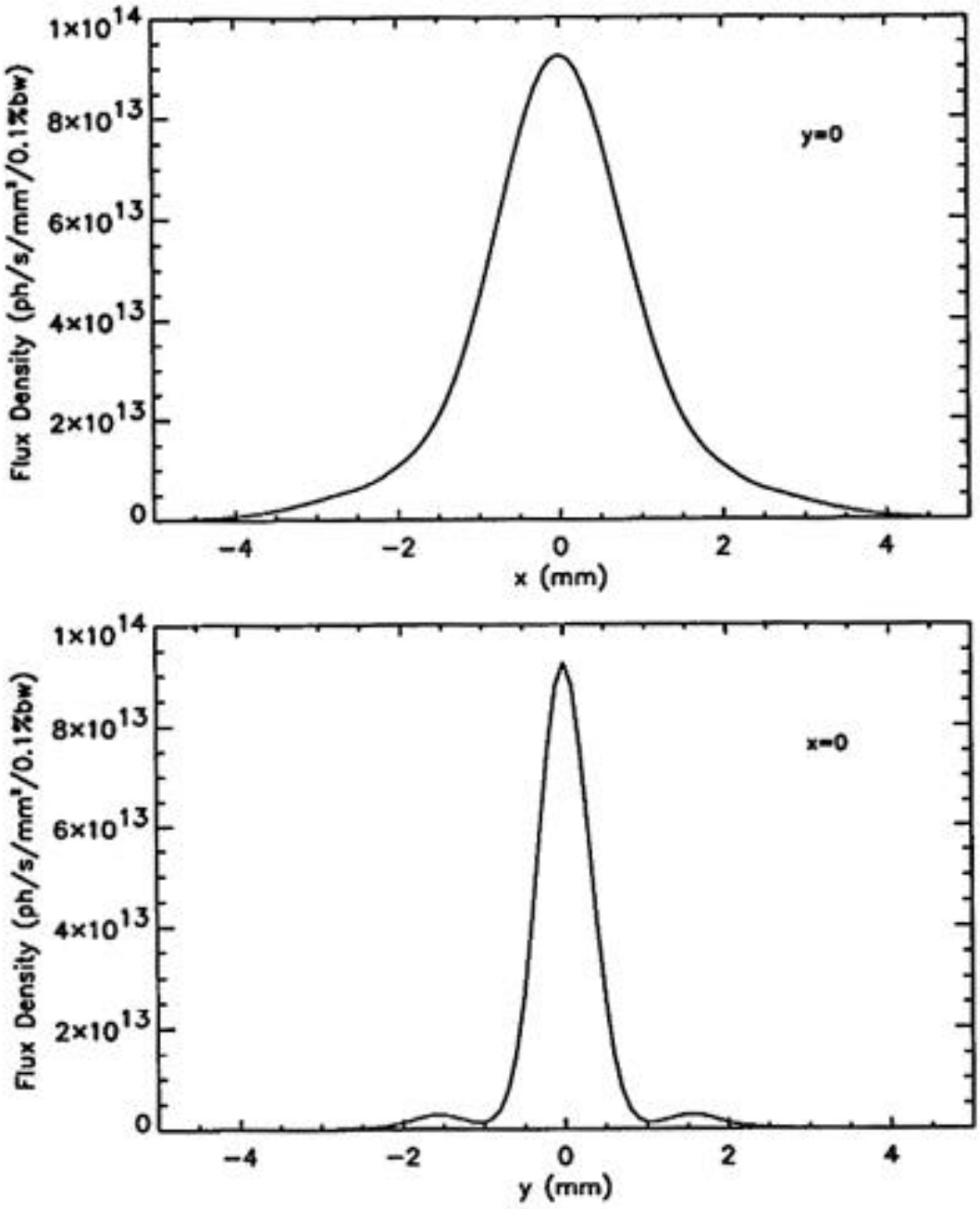

Figure 8d. Flux density cross-section profiles in the horizontal and vertical directions at the *third* harmonic energy (24.18 keV). The $FWHM_x$ is 1.92 mm, and the $FWHM_y$ is 0.74 mm.

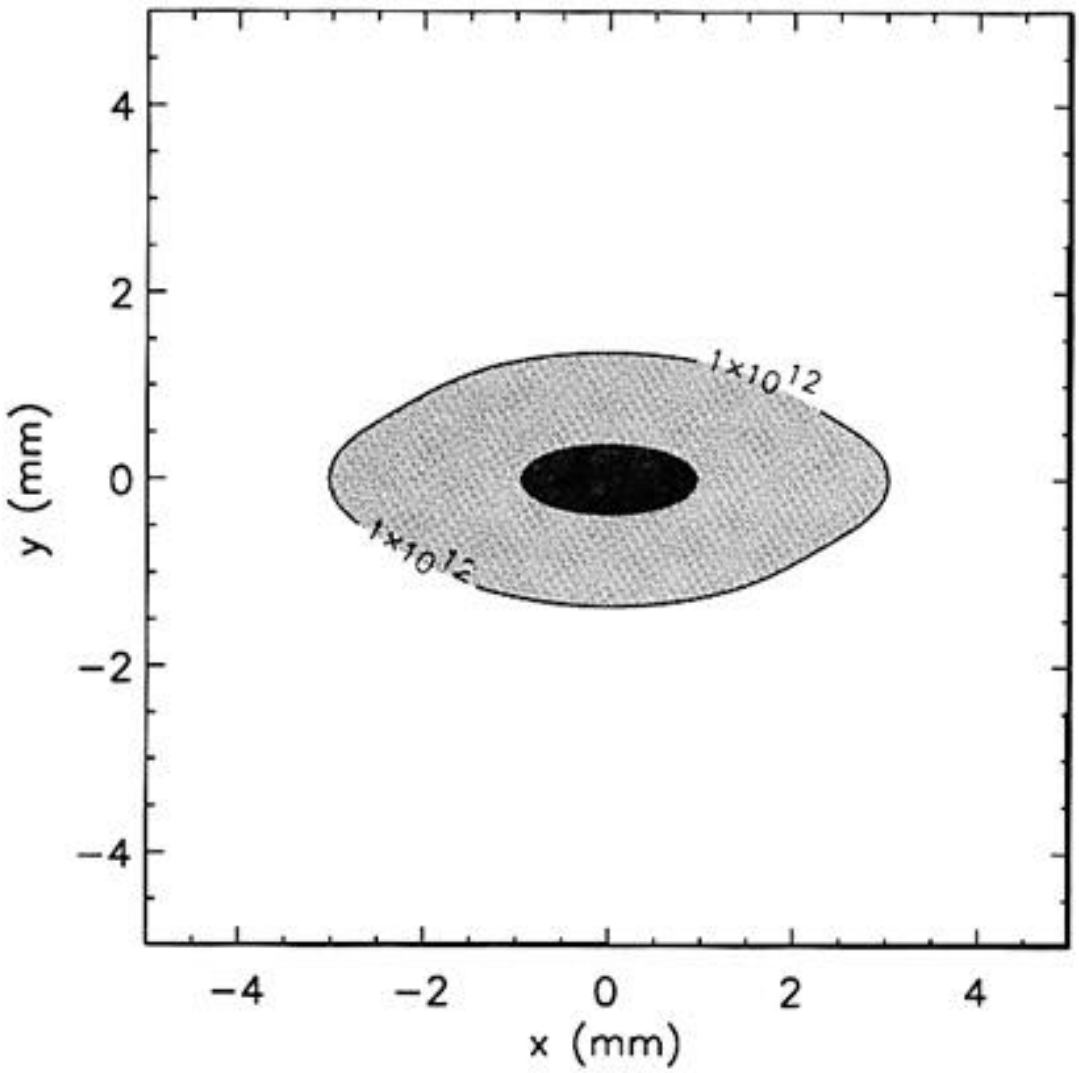

Figure 8e. Spatial photon distribution at 30.0 m from the source for K_{eff} = 1.22 (gap 17.8 mm) at the *fifth* harmonic energy (40.35 keV). The peak intensity is 2.64 x 10^{13} ph/s/mm^2/0.1%bw.

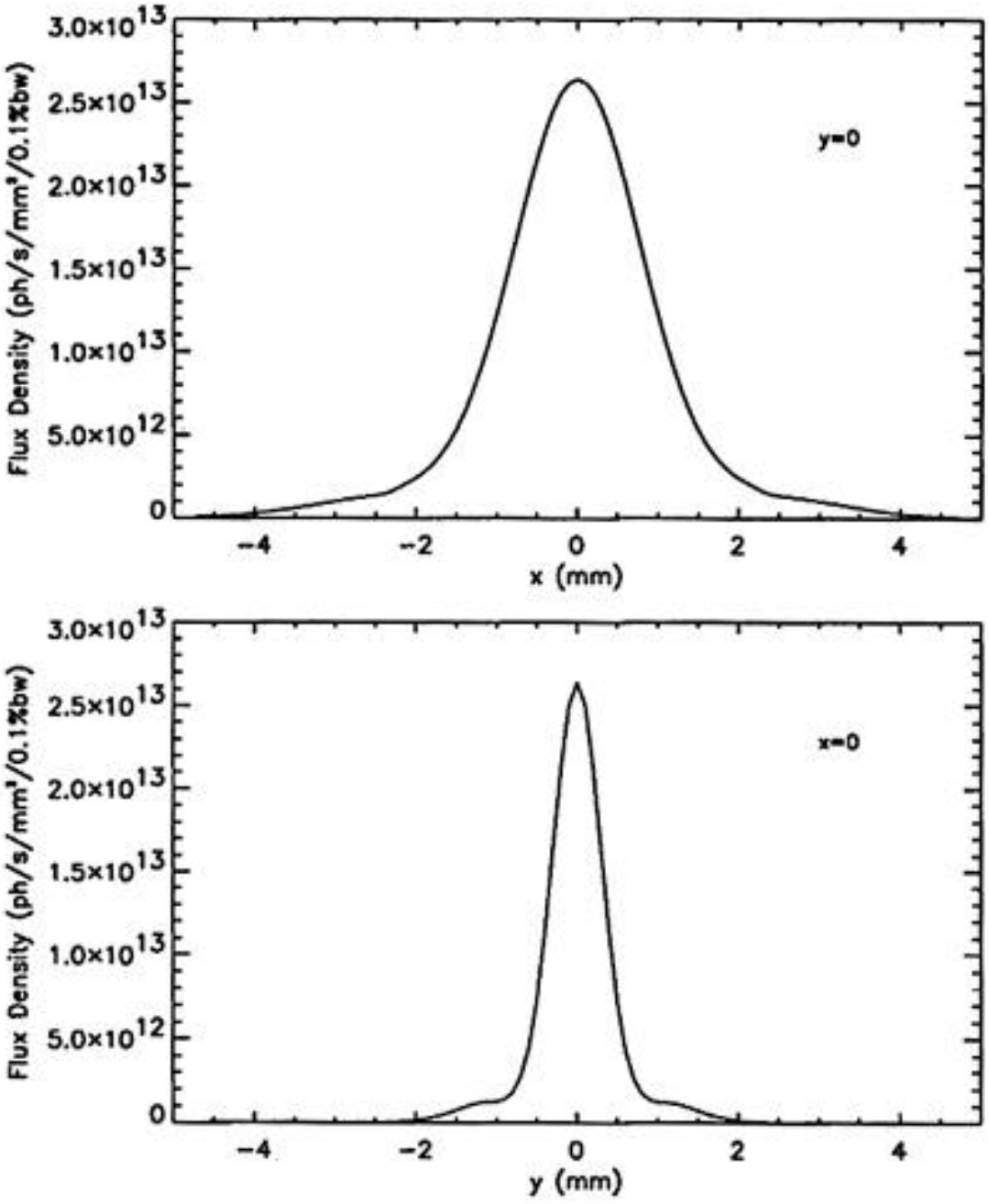

Figure 8f. Flux density cross-section profiles in the horizontal and vertical directions at the *fifth* harmonic energy (40.35 keV). The $FWHM_x$ is 1.90 mm, and the $FWHM_y$ is 0.72 mm.

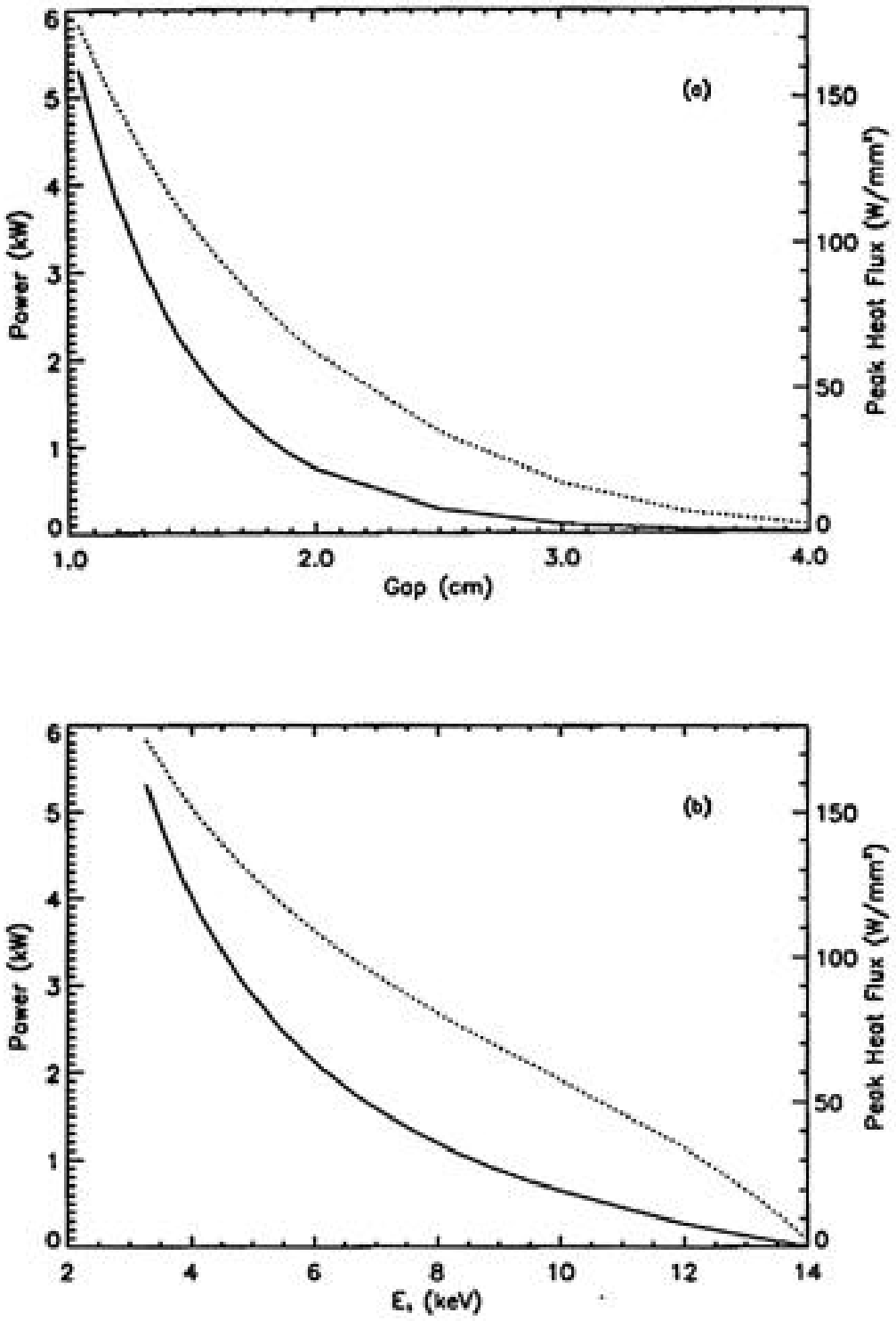

Figure 9. a) Total emitted power (solid) and peak heat flux at normal incidence (dotted) at 30.0 m from the source vs. gap using B_{peak} listed in Table 2 for the calculations. b) Same as a) except plotted vs. energy of the first harmonic.

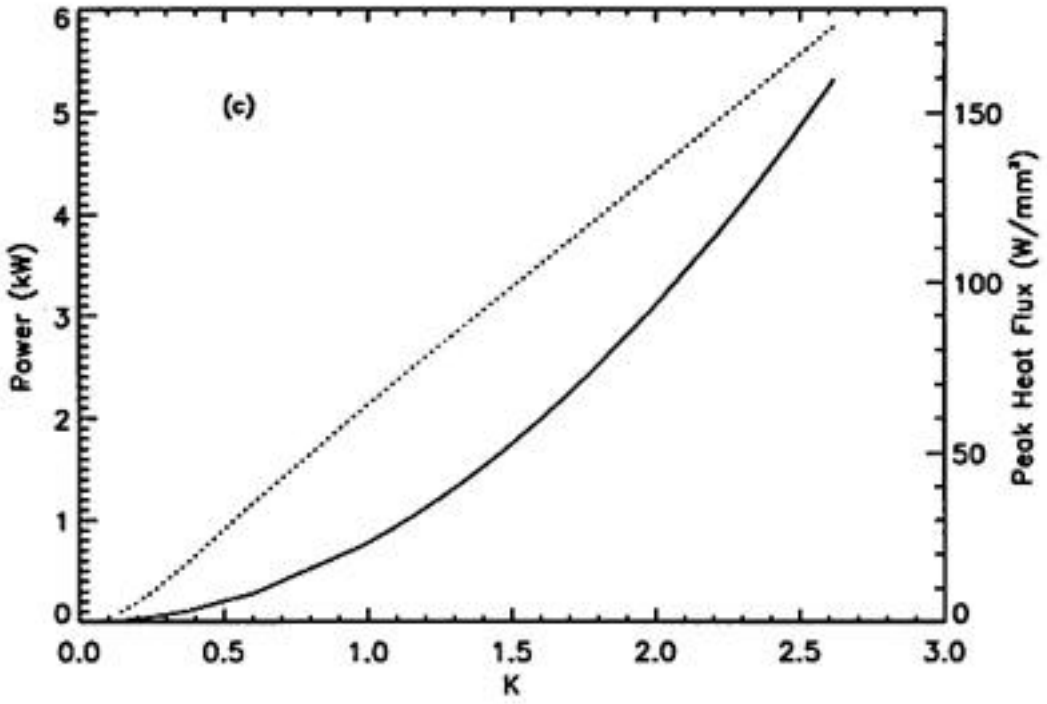

Figure 9. c) Total emitted power (solid) and peak heat flux at normal incidence (dotted) at 30.0 m from the source vs. K (derived from the B_{peak} listed in Table 2). For K > 1, the peak heat flux may be approximated by a straight line with a slope of 70 W/mm^2.

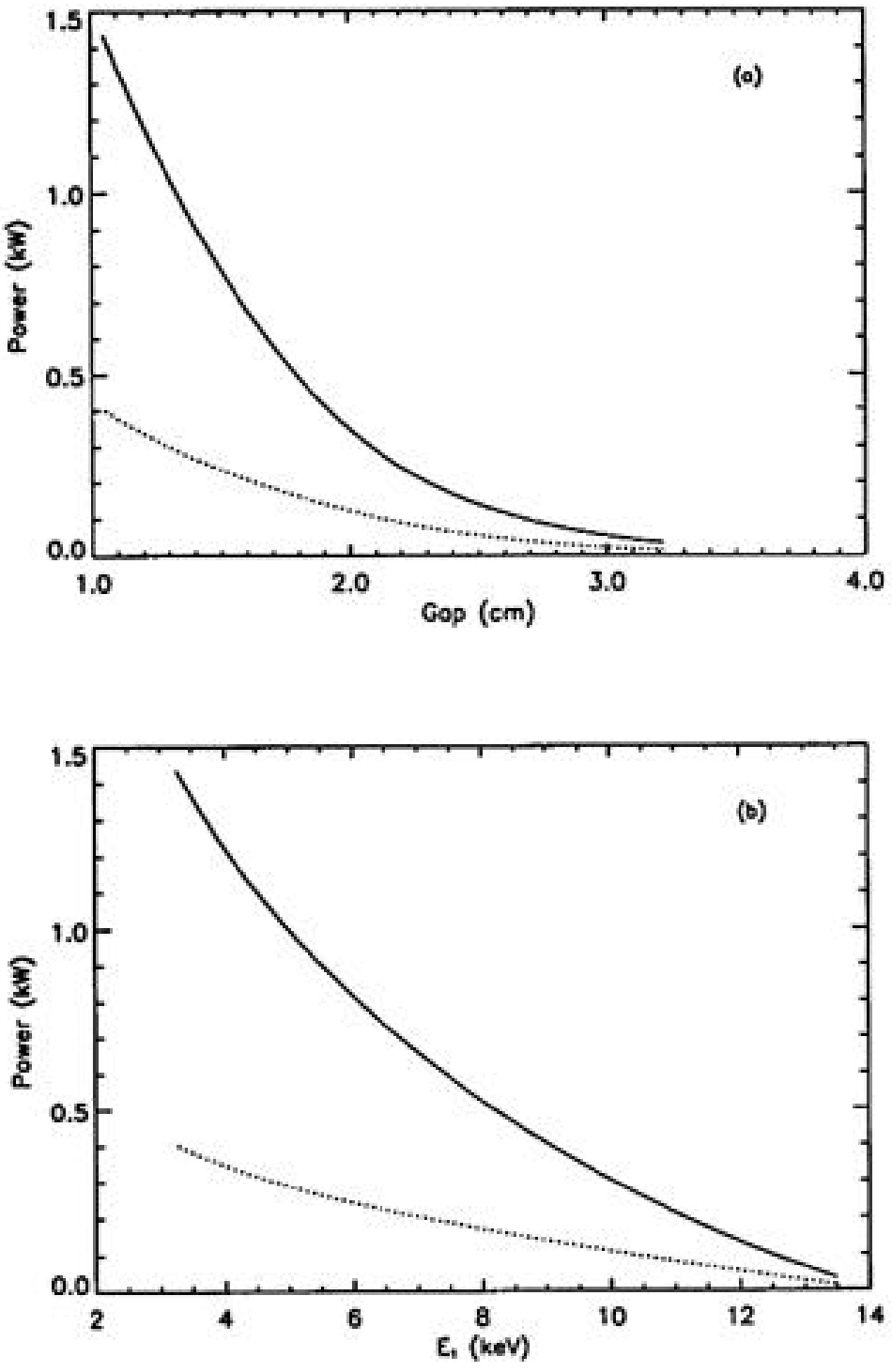

Figure 10. a) Transmitted power through a 5.0 mm x 2.0 mm (solid) and a 2.5 x 1.0 mm (dotted) aperture at 30.0 m from the osurce plotted vs. gap. b) Same as a) except plotted vs. energy of the first harmonic.

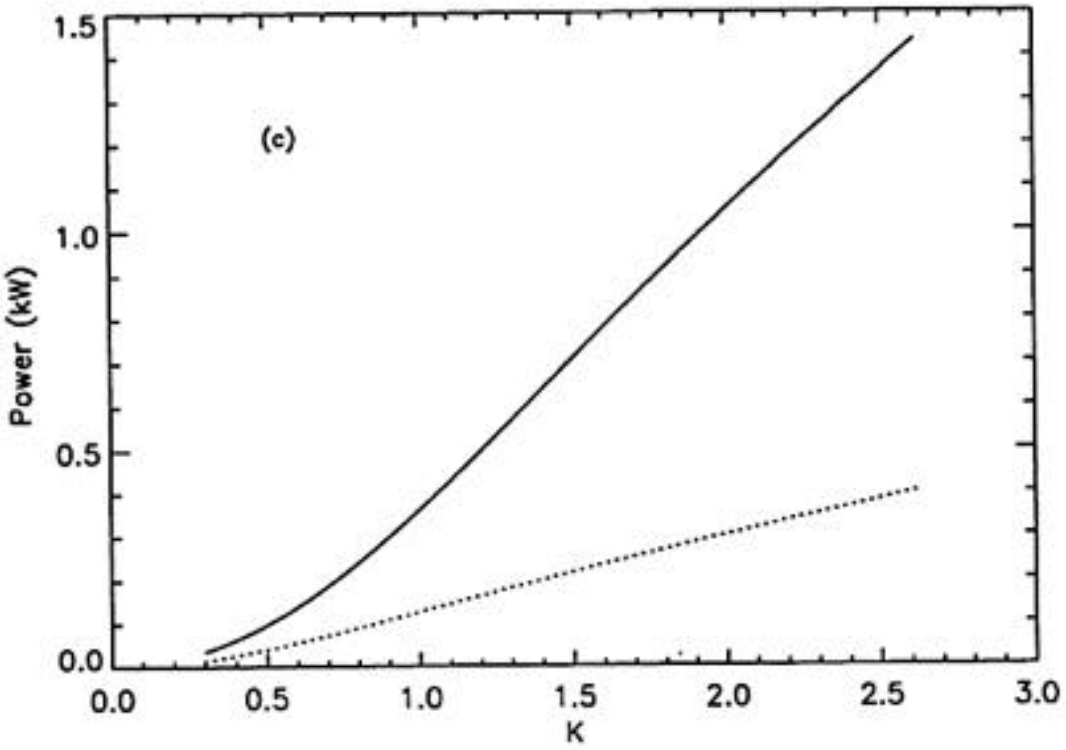

Figure 10. c) Transmitted power through a 5.0 mm x 2.0 mm (solid) and a 2.5 x 1.0 mm (dotted) aperture at 30.0 m from the source as a function of K. For K > 1, the power may be approximated by straight lines with slopes 670 W (solid) and 170 W (dotted). The transmitted power scales approximately linearly with the area of the aperture.

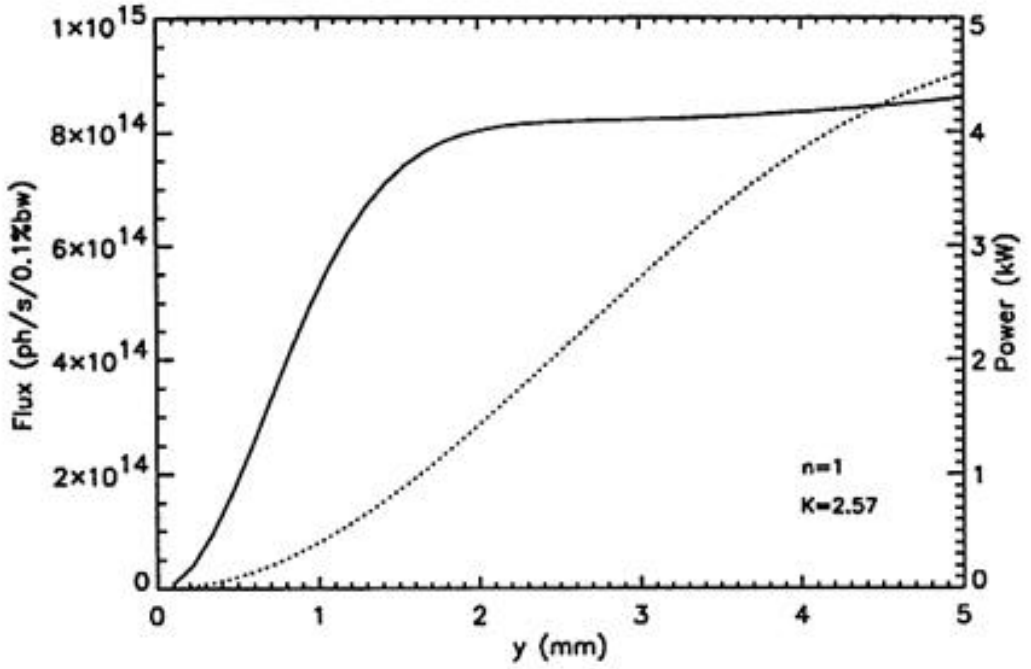

Figure 11. Transmitted flux (solid) and power (dotted) vs. vertical size of aperture (horizontal size is 2.5 x vertical size) at 30.0 m from the source for a closed gap (10.5 mm, K_{eff} = 2.57) at the first harmonic energy (3.25 keV). Only the first harmonic (n=1) provides flux at this energy.

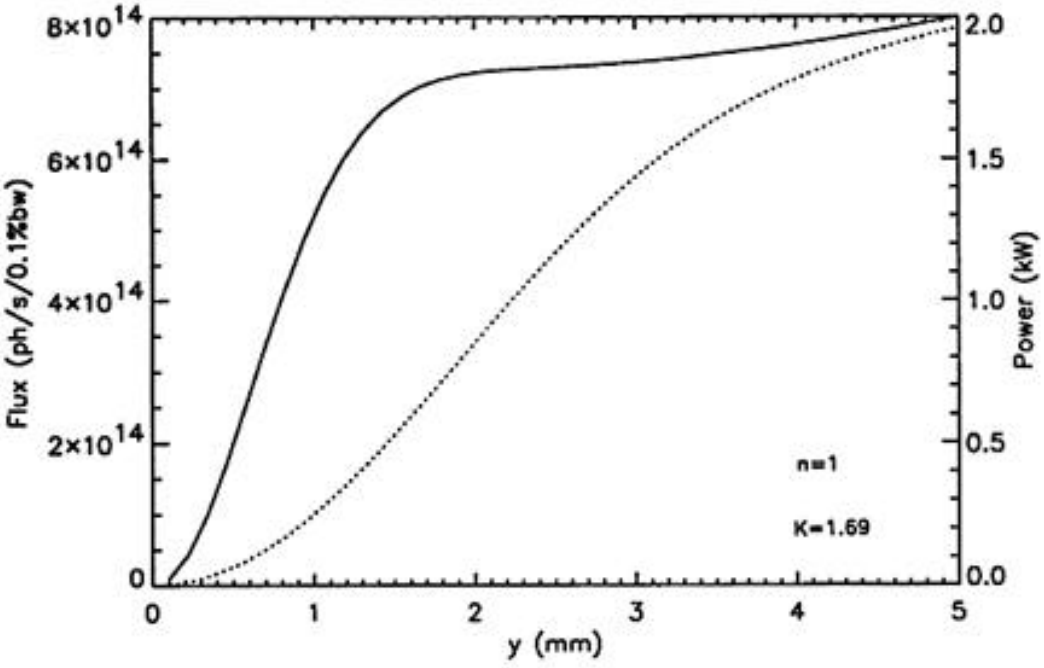

Figure 12. Transmitted flux (solid) and power (dotted) vs. vertical size of aperture (horizontal size is 2.5 x vertical size) at 30.0 m from the source for a gap of 14.5 mm (K_{eff} = 1.69) at the first harmonic energy (5.76 keV). Only the first harmonic (n=1) provides flux at this energy.

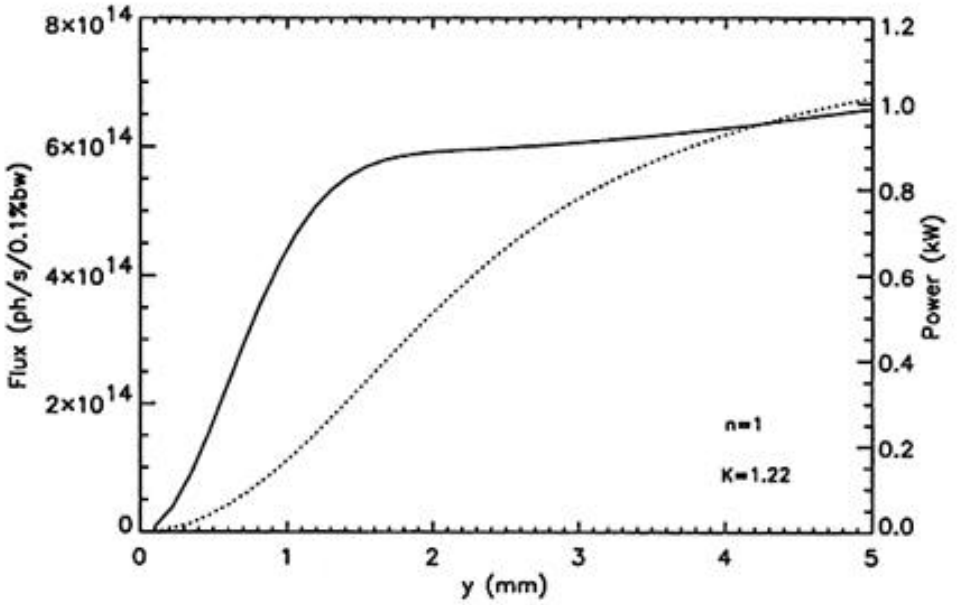

Figure 13. Transmitted flux (solid) and power (dotted) vs. vertical size of aperture (horizontal size is 2.5 x vertical size) at 30.0 m from the source for a gap of 17.8 mm (K_{eff} = 1.22) at the first harmonic energy (8.01 keV). Only the first harmonic (n=1) provides flux at this energy.

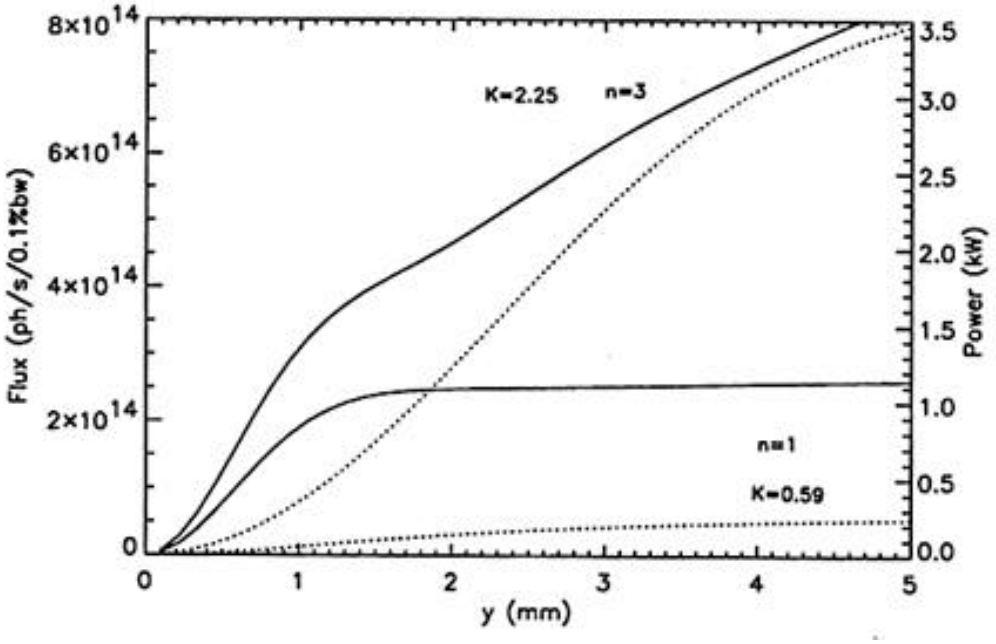

Figure 14. Transmitted flux (solid) and power (dotted) vs. vertical size of aperture (horizontal size is 2.5 x vertical size) at 30.0 m from the source at 12.0 keV). The first harmonic (n=1, K_{eff} = 0.59) provides a smaller flux than the third harmonic (n=3. K_{eff} = 2.25) but also substantially smaller power.

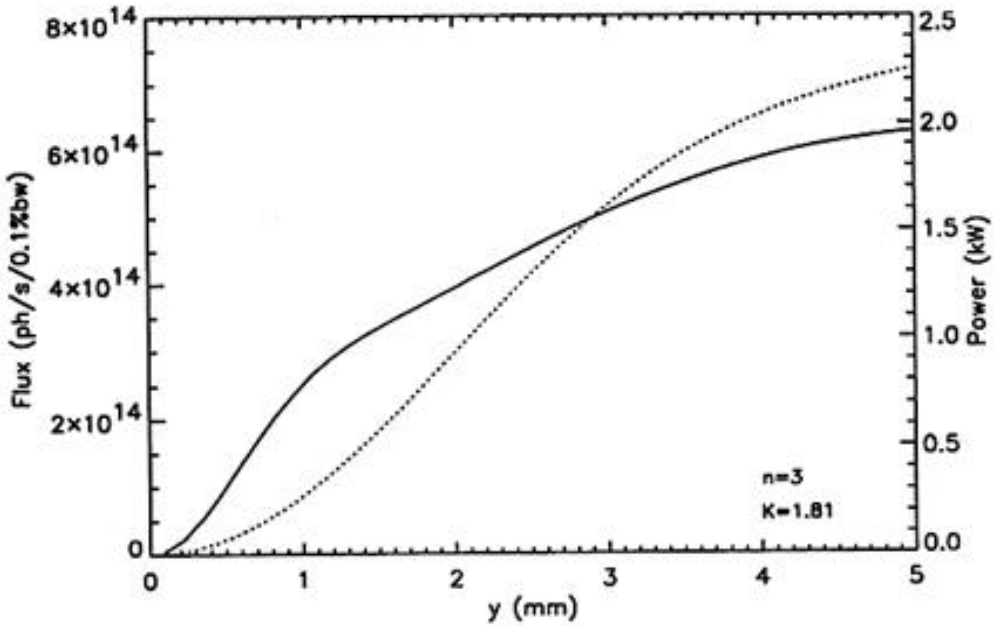

Figure 15. Transmitted flux (solid) and power (dotted) vs. vertical size of aperture (horizontal size is 2.5 x vertical size) at 30.0 m from the source at 16.0 keV (K_{eff} = 1.81). Only the third harmonic (n=3) provides a large flux at this energy.

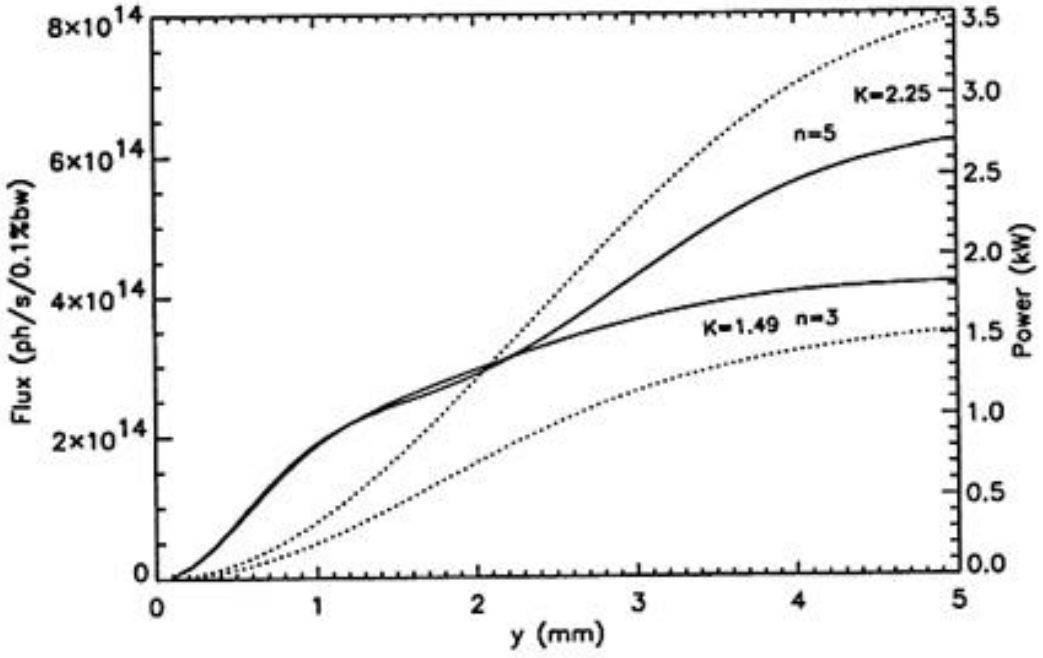

Figure 16. Transmitted flux (solid) and power (dotted) vs. vertical size of aperture (horizontal size is 2.5 x vertical size) at 30.0 m from the source at 20.0 keV. The third harmonic (n=3, K_{eff} = 1.49) provides about the same flux as the fifth harmonic (n=5, K_{eff} = 2.25) but substantially smaller power.

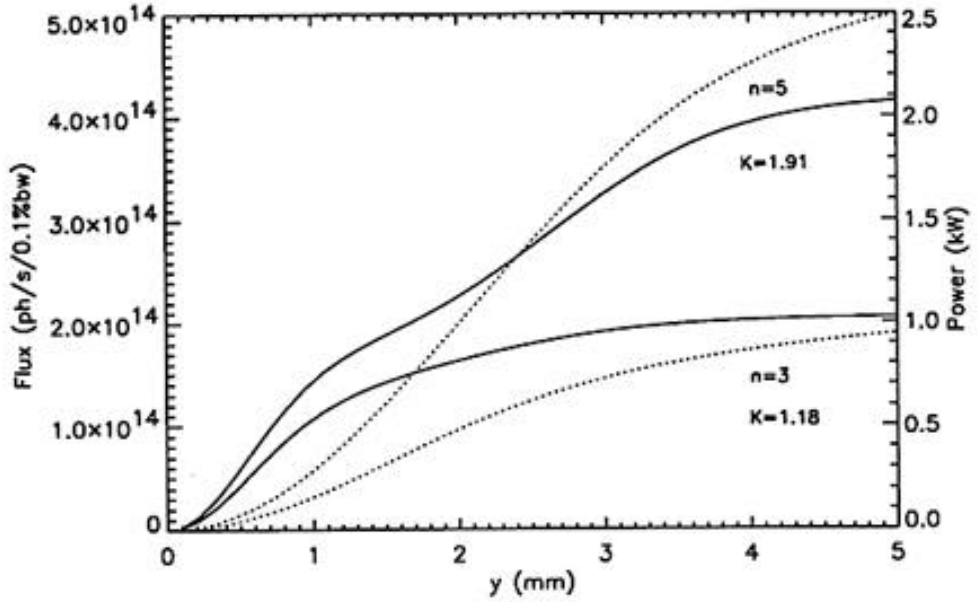

Figure 17. Transmitted flux (solid) and power (dotted) vs. vertical size of aperture (horizontal size is 2.5 x vertical size) at 30.0 m from the source at 25.0 keV. The third harmonic (n=3, K_{eff} = 1.18) provides a smaller flux than the fifth harmonic (n=5, K_{eff} = 1.91) but also substantially smaller power.

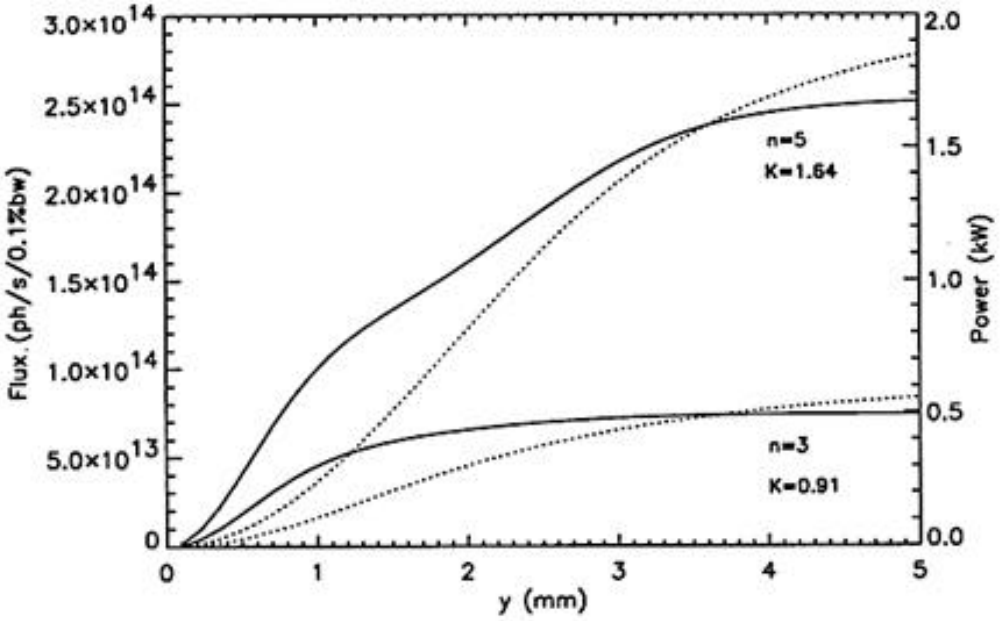

Figure 18. Transmitted flux (solid) and power (dotted) vs. vertical size of aperture (horizontal size is 2.5 x vertical size) at 30.0 m from the source at 30.0 keV. The third harmonic (n=3, K_{eff} = 0.91) provides a smaller flux than the fifth harmonic (n=5, K_{eff} = 1.64) but also substantially smaller power.

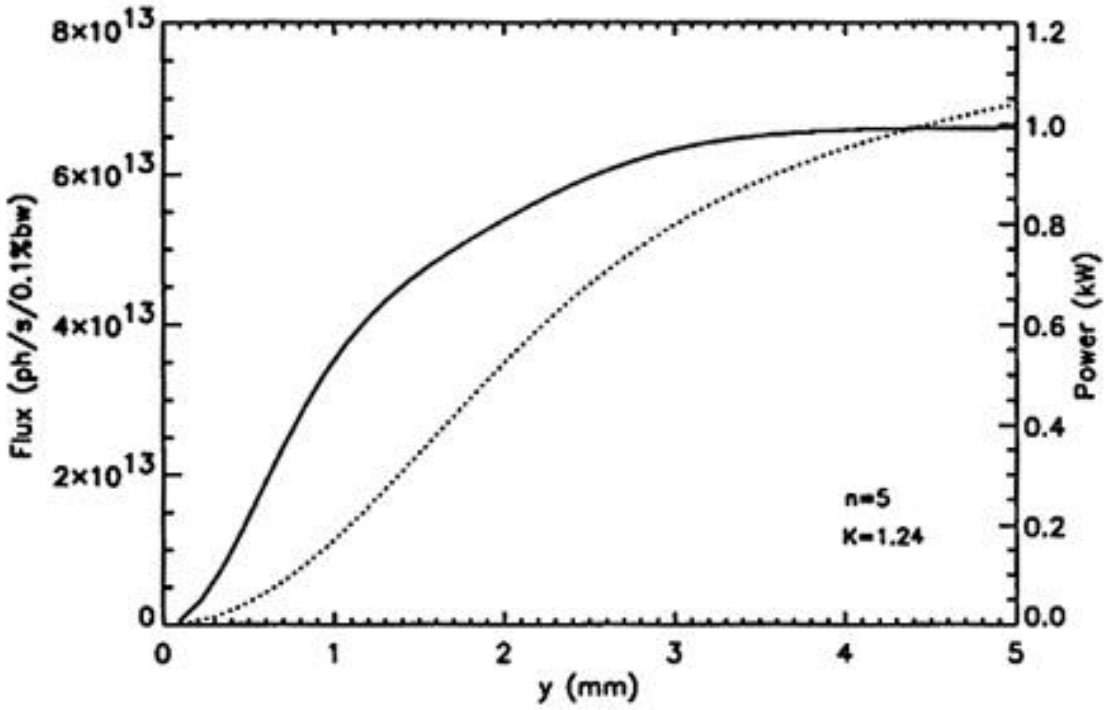

Figure 19. Transmitted flux (solid) and power (dotted) vs. vertical size of aperture (horizontal size is 2.5 x vertical size) at 30.0 m from the source at 40.0 keV (K_{eff} = 1.24). Only the fifth harmonic (n=5) provides a large flux at this energy.

Appendix

Storage Ring Parameters

We have used revised values for the APS beam parameters in this document. For the APS, the radiation characteristics are dominated by the emittance of the stored positron beam. The horizontal (x) and vertical (y) emittances $\varepsilon_{x,y}$ are derived from the natural emittance. The nominal natural beam emittance ε for the APS is 8.2×10^{-9} m-rad and, by using the nominal value of 10% coupling, we have

$$\varepsilon_x = 7.45 \times 10^{-9} \text{ m-rad}$$

$$\varepsilon_y = 7.45 \times 10^{-10} \text{ m-rad}$$

for the emittance in the two directions.

For all practical calculations, the beam size and beam divergence may be determined from the β-functions at the center of the straight section. The insertion device is located off-center by 1.25 m, but the variation of β is small and may be ignored. Further, the dispersion in the straight section is also small and can be omitted. The beam parameters are therefore derived from

$$\sigma_x = \sqrt{\varepsilon_x \beta_x}, \qquad \sigma_{x'} = \sqrt{\varepsilon_x / \beta_x},$$

$$\sigma_y = \sqrt{\varepsilon_y \beta_y}, \qquad \sigma_{y'} = \sqrt{\varepsilon_y / \beta_y}.$$

By inserting the nominal values $\beta_x = 14.2$ m and $\beta_y = 10.0$ m, we have

$$\sigma_x = 325 \text{ μm}, \qquad \sigma_{x'} = 23 \text{ μrad},$$

$$\sigma_y = 86 \text{ μm}, \qquad \sigma_{y'} = 9 \text{ μrad}.$$

With regards to earlier published beam parameters, the current values are slightly different. In comparison with those found in ANL-88-9, the β_x has changed from 13.0 m to 14.2 m, and the natural emittance ε has changed from 8.0×10^{-9} m-rad to 8.2×10^{-9} m-rad. The ANL/APS/TB-3 listed different values for the horizontal and vertical beam emittances with small changes for the derived beam parameters. The revised values of the APS source parameters are summarized in Table A1.

Phase Space

The x-ray photon beam has an inherent beam size σ_r and a divergence $\sigma_{r'}$ given by

$$\sigma_r = \frac{\sqrt{2\lambda L}}{4\pi} \qquad \sigma_{r'} = \sqrt{\frac{\lambda}{2L}},$$

where λ is the wavelength of the emitted radiation, and L is the length of the insertion device. These equations have been corrected and include now a factor of the square root of two in the definitions that was omitted in TB-3, Eq. 6. The diffraction-limited source size σ_r has no effect on the radiation for the APS, and the diffraction-limited source divergence $\sigma_{r'}$ makes a significant contribution only at low energies as is indicated in Figure A1, which shows the total source size $\Sigma_{x,y}$ and the total source divergence $\Sigma_{x',y'}$ as a function of energy. The phase space of the undulator radiation is therefore characterized by

$$\Sigma_{x,y} = \sqrt{\sigma_{x,y}^2 + \sigma_r^2}, \qquad \Sigma_{x',y'} = \sqrt{\sigma_{x',y'}^2 + \sigma_{r'}^2}.$$

Distance Scaling

The effective beam divergence scales approximately linearly with the distance from the source. A second-order correction may be obtained by noting that, in a Gaussian approximation, the source size $\Sigma_{x,y}$ contributes approximately a term $\frac{\Sigma_{x,y}}{D}$ to the source divergence at the distance D. For the APS, the contribution is less than 10% in the horizontal plane (< 2 μrad) and less than 5% in the vertical plane (< 0.5 μrad) at 30.0 m. The correction factor is obtained from

$$\Sigma_{Tx',y'}(D) = \sqrt{\Sigma_{x',y'}^2 + \left(\frac{\Sigma_{x,y}}{D}\right)^2},$$

where $\Sigma_{Tx',y'}(D)$ is an estimate of an effective source divergence at distance D ($\Sigma_{x,y}$ can be replaced by $\sigma_{x,y}$ for the APS.)

The distance-scale factor for an observation point at distance D_2 is therefore

$$S(D_2) = \left(\frac{D_2}{D_1}\right) \frac{\Sigma_{Tx',y'}(D_2)}{\Sigma_{Tx',y'}(D_1)}$$

when the radiation pattern is known at distance D_1 (30.0 m). Thus, this scale factor may be used to estimate spatial distributions at distances other than 30.0 m. The peak intensity scales as S^{-2}.

Table A1. Source parameters for undulator A

Parameter	**Value**
Storage ring energy	7.0 GeV
Storage ring current	100 mA
Natural beam emittance, ε	8.2×10^{-9} m-rad
Coupling constant	10%
Horizontal beam emittance, ε_x	7.45×10^{-9} m-rad
Vertical beam emittance, ε_y	7.45×10^{-10} m-rad
Horizontal beta-function (center of straight section), β_x	14.2 m
Vertical beta-function (center of straight section), β_y	10.0 m
Horizontal beam size, σ_x	325 µm
Vertical beam size, σ_y	86 µm
Horizontal beam divergence, $\sigma_{x'}$	23 µrad
Vertical beam divergence, $\sigma_{y'}$	9 µrad

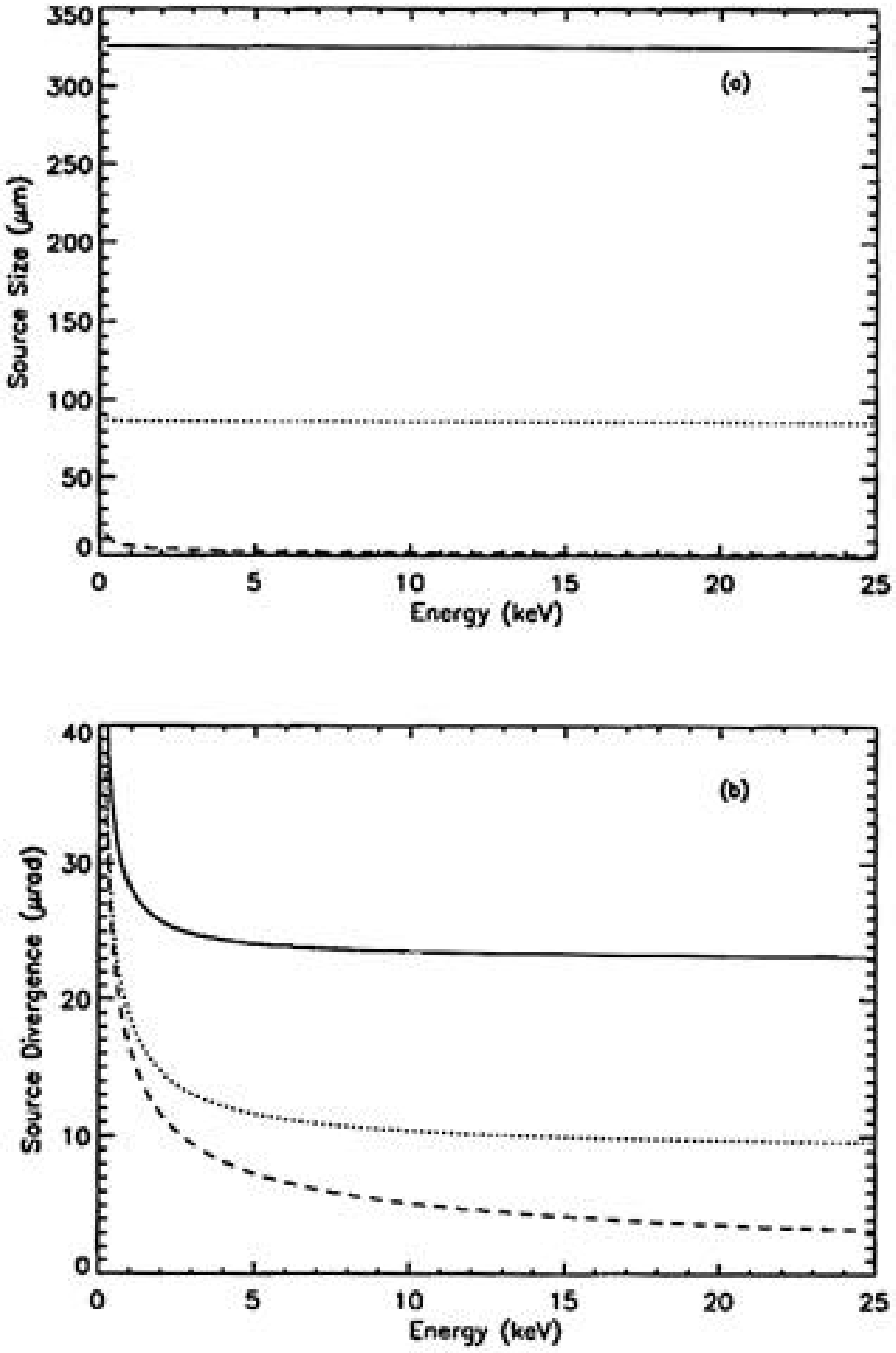

Figure A1. a) Total source size as a function of energy. Σ_x (solid), Σ_y (dotted), and σ_r (dashed). b) Total source divergence vs. energy. $\Sigma_{x'}$ (solid), $\Sigma_{y'}$ (dotted), and $\sigma_{r'}$ (dashed).